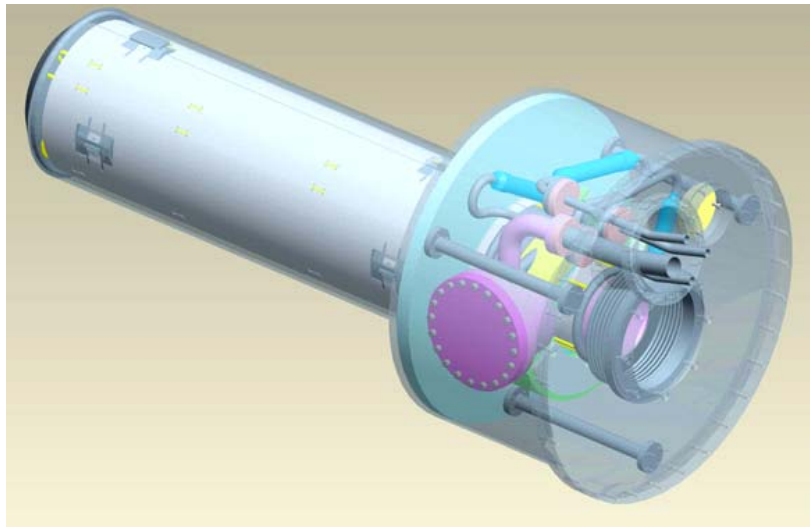
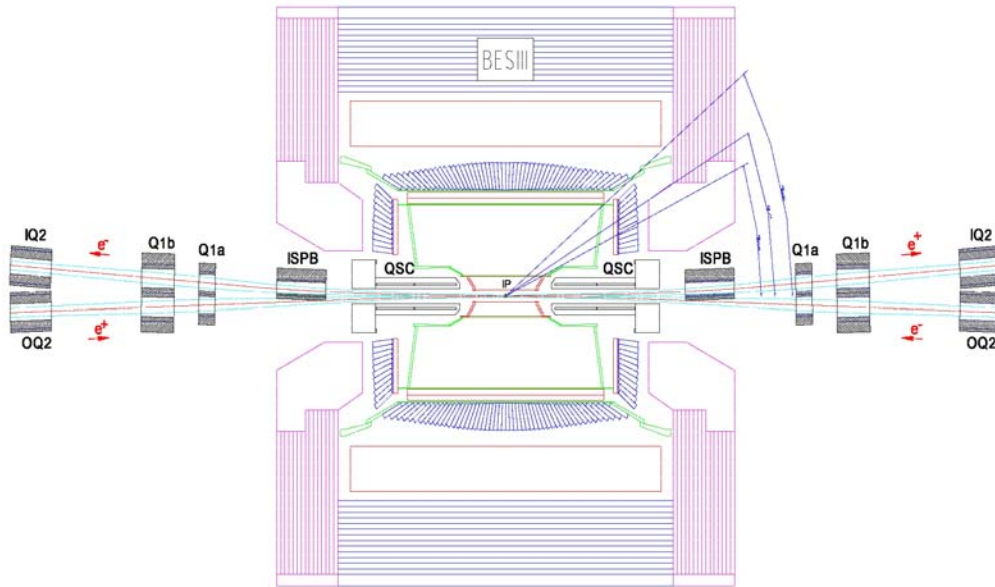


Design Report for the BEPC-II Superconducting IR Magnets



Design Report for the BEPC-II Superconducting IR Magnets

1. Introduction	4
2. Superconducting Coil Fabrication Technique	6
3. Superconducting Coil Geometry and Layout	10
4. Collider and Synchrotron Radiation Mode Design Considerations	14
5. Cold Mass Forces and Torques Due to the BES-III Solenoid	17
6. Overview of Mechanical Design	21
7. Pressure Vessel and Safety Certification	22
Inner Cryostat Vessel (21010016).....	23
Inner Helium Vessel (21010017)	24
Helium Outer Vessel (21010020).....	25
Outer Cryostat Vessel (21010015)	26
Cryostat End Volume Housing (21010010).....	27
Lead Box Bottom Flange (21010025)	28
Lead Wiring Box Housing (21010024).....	29
Pressure Leak Testing	30
8. Cold Mass Heat Leak Calculations at 4°K	31
Conduction and Radiation From 80K.....	32
Conduction and Radiation From 300K	34
Conduction From Key Support.....	35
Conduction Through Axial Support.....	37
Total Heat Load to 4 K System.....	38
9. 3D Structural Analysis	39
Axial Restraint	39
Key Support Stress.....	41
10. Magnet Interface	42
11. Open Issues	44
Appendix 1. SCQ Quench Protection Design Study Comparison	45
Appendix 2. Power Supply, Instrumentation and Quench Protection Considerations	50
Appendix 3. Drawing Package and Parts List	54

1. Introduction

This Design Report, produced under the Inter-Laboratory Collaborative Agreement between IHEP and BNL as specified in Attachment #1 to the IHEP-BNL Memorandum of Understanding, describes the design, fabrication and quality assurance requirements for the superconducting micro-beta quadrupole magnet package for use in the BEPC-II upgrade. BEPC-II is an upgrade project to BEPC, the Beijing Electron Positron Collider. It is designed not only as an electron-positron collider in the energy range of 1.55 GeV to 1.89 GeV, but also as a dedicated synchrotron radiation facility at an energy of 2.5 GeV.

In order to meet the machine requirements, a multi-purpose superconducting (SC) magnet will be used on each side of the interaction point (IP). The magnet consists of a magnet package and a magnet cryostat. The magnet package includes an anti-solenoid (AS), a final focusing quadrupole (SCQ), a bending dipole (SCB), a vertical dipole corrector and a skew quadrupole corrector. They are contained in a common cryostat which constrains motion during cooling down and excitation. The BES-III detector together with the accelerator components on each side of the IP is shown in Figure 1.1. Since the SC magnets are installed completely inside the BES-III detector and operated in the detector solenoid field of 1.0 T, they must be iron-free devices. Each magnet cryostat will be supported by a movable stage that is located outside the detector.

The magnetic design specifications given in this report have been determined by a collaborative effort between BNL and IHEP. The magnets will be built and initially tested at BNL. This design report provides all the necessary information for other sub-system interfacing to the magnet package. This includes operating parameters, mechanical dimensions, interface specifications, and electrical and cryogenic connections.

The design report describes the coil fabrication techniques, coil geometries and forces and torques arising from the interaction with external magnetic fields. A mechanical

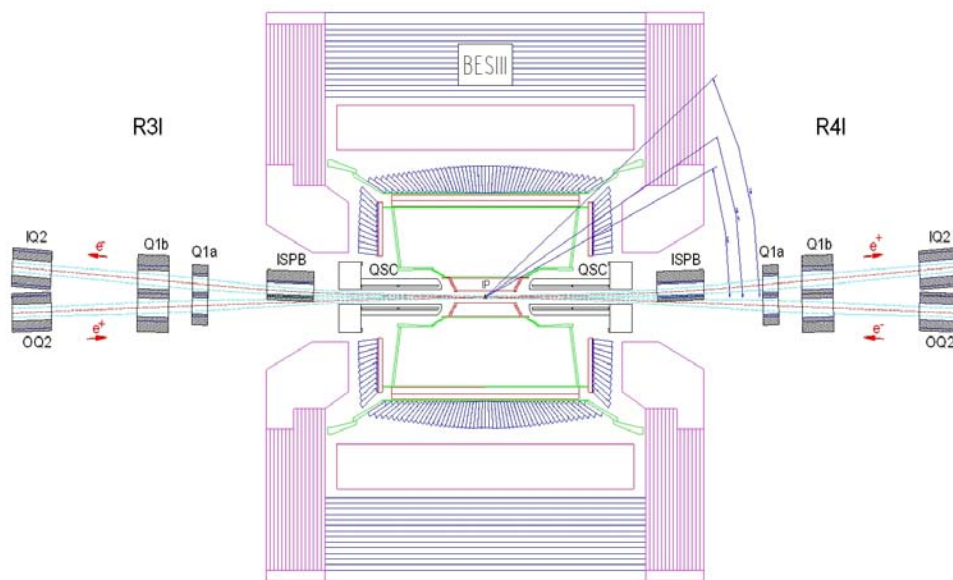


Figure 1.1: Top View of the BES-III Detector and IP Accelerator Components.

design description includes an overview, a pressure vessel analysis, a heat load and structural analysis. The report also outlines the remaining open design issues. A drawing package and part list based on a 3D solid model is also included with this report.

While not strictly part of the design report, BNL has previous experience with similar systems in different accelerator facilities. Based on this experience the design report includes as appendices details of the quench protection design study together with conceptual power supply, instrumentation and quench protection systems. These sections are of a more generic nature and are intended to guide the designs of these systems rather than specify them.

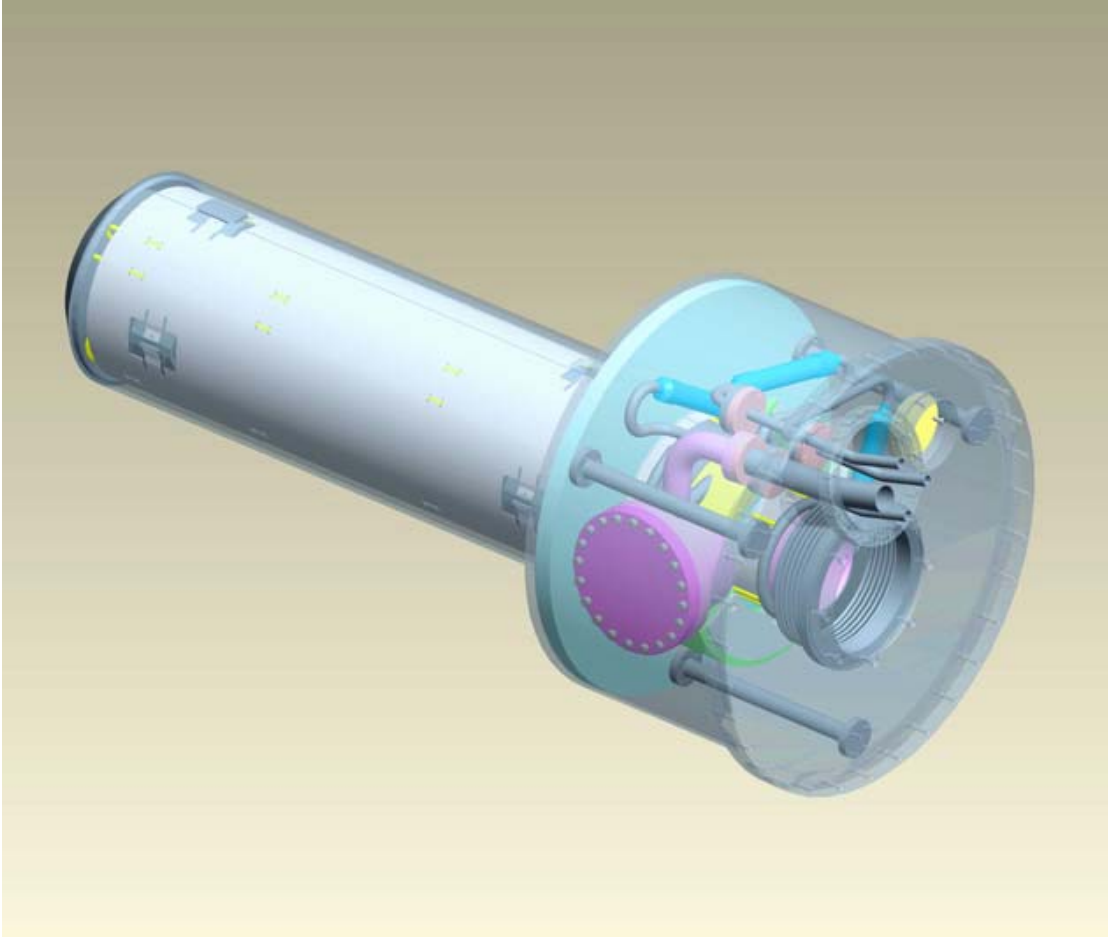


Figure 1.2: BEPC-II Superconducting IR Magnet 3-D Mechanical Model, non-IP End Isometric. *The outer shells are shown translucent for clarity.*

2. Superconducting Coil Fabrication Technique

The manufacturing of the BEPC-II magnet coils will be done using the direct wind technology developed within the BNL Superconducting Magnet Division. This manufacturing process eliminates the wire placement errors due to transfer of pre-wound coil patterns onto a tube. It also compensates for potential wire placement errors due to variations in support tube diameter and straightness. Finally this process allows the flexible fabrication of relatively arbitrary coil patterns.

The first step in the manufacturing of the coils is the generation of the coil pattern to be placed onto the support tube. Patterns for each layer of the magnet are developed two layers at a time. Each coil of the magnet is a two-layer construction, using an impregnated fiberglass substrate on the bottom of each layer, and sandwiched in between the first and second layer of each coil.

Once a coil pattern is generated and checked using magnetic analysis software, the wiring file is loaded into the computer controller of the 11 axis winding machine, and the conductor is wound and ultrasonically welded onto the surface of the support tube. After full pattern completion, the support tube is then measured warm to determine the field accuracy of the just finished winding. During a warm field measurement at low current, the harmonics of the resultant coil are determined. In the case of a multi-layer magnet, such as the main quad magnet for BEPC, the harmonic measurements will be used to determine corrections to be introduced into the next layer of the magnet. This is done at the winding machine, where the winding software has provisions for modulating a coil pattern to provide desired harmonics.

After a coil layer is complete, and magnetically acceptable, it is then overwrapped with impregnated fiber-glass and cured in an oven. The fiber-glass, when cured, is capable of withstanding the magnetic forces resulting from the excitation currents within the final application. After curing, the support tube is placed back onto the winding machine for the next layer of the magnet.

An example of a double-layer quadrupole winding is shown in Figure 2.1 where the

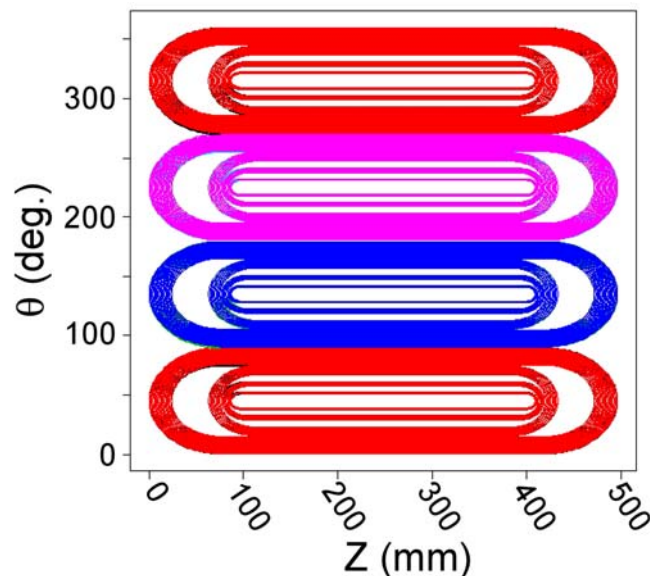


Figure 2.1: Sample Double Layer Quadrupole Coil Winding Pattern.

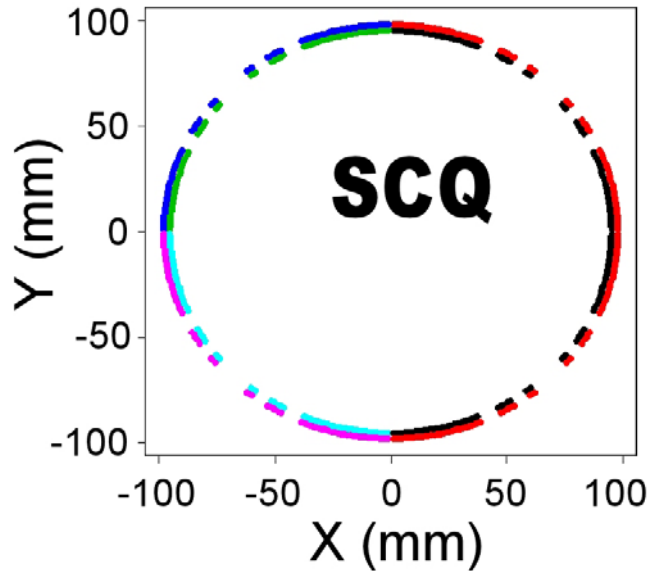


Figure 2.2: Sample Double Layer Quadrupole Coil Cross Section.

coil pattern is shown unwrapped from the tube and Figure 2.2 which shows the 2D coil cross-section in the middle of the magnet. This quadrupole pattern has four poles, where there is no conductor, at $\theta = 45, 135, 225$ and 315 degrees along with empty sections running along the pattern's straight section to adjust 2D (body) harmonics and empty spaces at each end to adjust end (integral) harmonics.

For this pattern winding starts at a coil midplane near 90° and proceeds inward in a clockwise fashion until the innermost turn at the pole is reached. Then winding stops so that precut G10 filler pieces can be filled in the gaps and a layer of substrate added so that winding can continue for the second layer of this pole. For the second layer winding continues in a clockwise manner this time working outward from the pole back to the midplane. Once the second layer of the first pole is complete we drop back down to the original first layer and continue with winding the first layer of the second pole at 135° but this time winding inward in a counterclockwise manner. When completed the gaps in this bottom layer pole are filled in as before and counterclockwise winding continues back outward from the second layer pole. This process is continued in the same manner for the rest of the poles with winding alternating between clockwise and counterclockwise.

This winding procedure allows fabrication of a compact coil structure with leads exiting from the coil ends rather than the poles as were done for the HERA-II single layer coil windings. If instead of the proposed four double-layer design SCQ were to be wound as eight single layers, handling the leads inside the pole region for eight layers would be problematic during fiberglass wrapping and epoxy curing. Also by continuously winding all the poles contained in two layers in a single operation the number of conductor splices is reduced.

A drawback of the proposed procedure is however that winding is frequently interrupted in order to add G10 and new substrate at each pole. To this end we are investigating applicability of an alternate winding pattern in which all the conductor for a

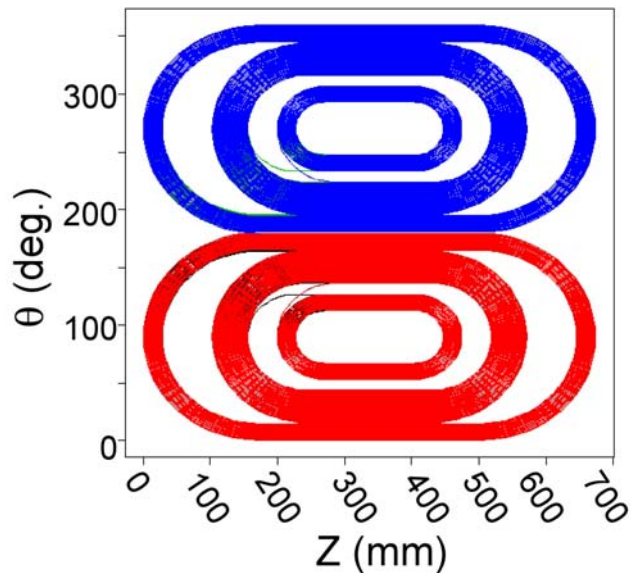


Figure 2.3: Sample Double Layer Dipole Coil Winding Pattern.

given winding layer is laid down at one time in a serpentine pattern before winding is interrupted to prepare G10 and substrate for winding the entire second layer. As of this writing winding tests with the new serpentine pattern style coils are just now being started and will be evaluated at a later time.

Figure 2.3 shows a double-layer winding pattern for the dipole coil, SCB. Note that much more space is needed for the SCB coil ends than that required for SCQ. In general dipole ends need to be almost twice as long as an equivalent radius quadrupole. So even though SCQ and SCB are intended to have the same magnetic length, 400 mm, we see that

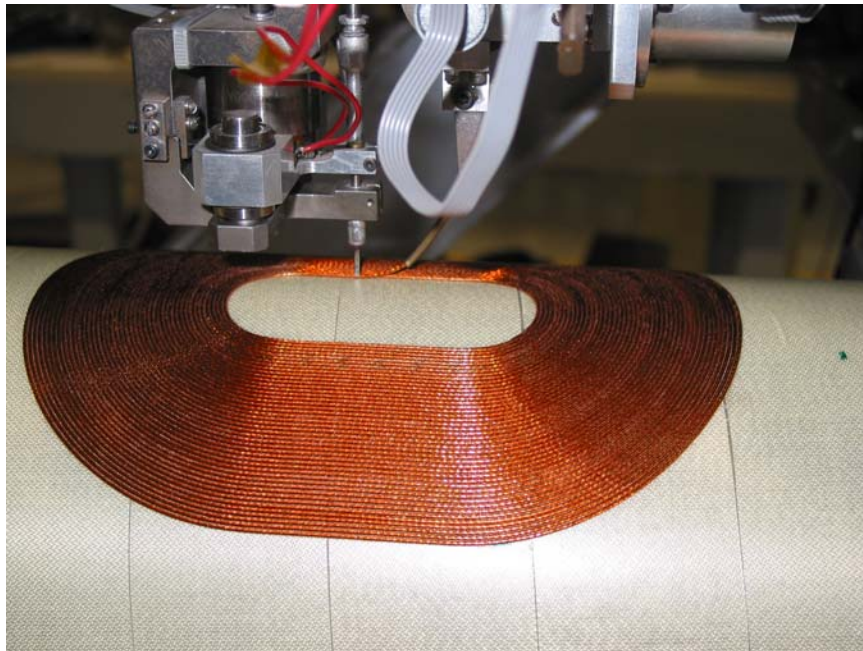


Figure 2.4: BEPC-II Test Coil Winding In Progress.

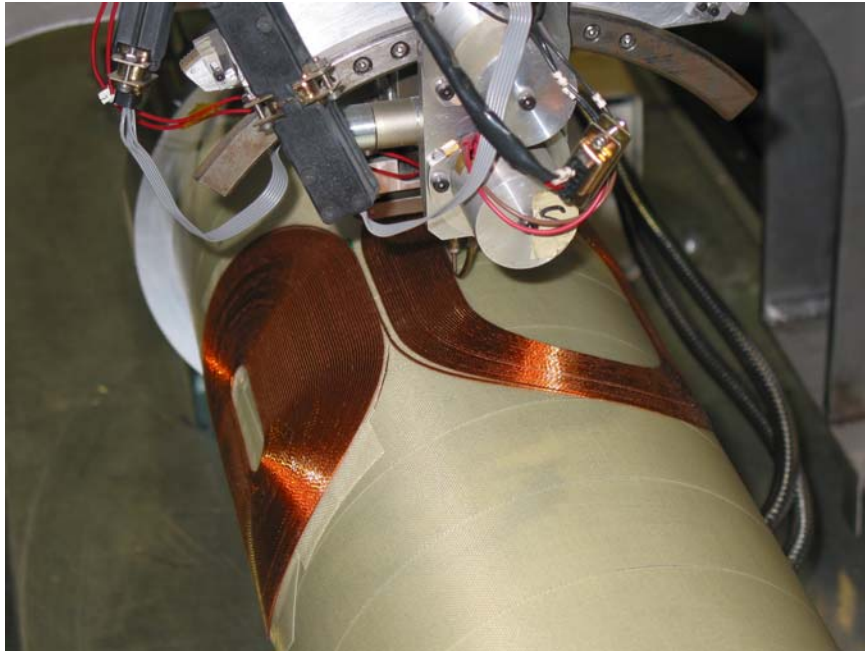


Figure 2.5: BEPC-II Test Coil Winding In Progress..

the 674 mm physical coil length for SCB is 178 mm longer than the 496 mm physical length for SCQ. In effect even though SCQ is shorter than SCB, SCQ has more “straight section length” and there is very little effect from the coil ends on the transfer function at the middle of the magnet. Counter wise SCB and VDC have significant contributions from the coil ends to their mid-point field, which must be taken into account when harmonic optimization is done.

Winding tests have been performed on a support tube of the correct diameter. The results are shown in Figure 2.4 and Figure 2.5. The first test pattern is a 52 turn per layer quadrupole. This is the first Research and Development trial using the two layer approach with a layer of fiberglass substrate placed between layers of the same coil pattern.

The technique required the placement of a substrate layer immediately following the completion of a single layer of a pole. Once the substrate is put into place, the spiral out second layer of the pole is wound, followed immediately by the first layer of the next pole. Research and Development work continues on the smallest radius turn required for the final coil pattern and iteration of the process parameters.

3. Superconducting Coil Geometry and Layout

The main parameters for the superconducting coils are given in Tables 3.1 and 3.2 and outline schematically in Figure 3.1. The BEPC-II superconducting magnet has a multi-function coil pack consisting of independent quadrupole (SSQ), horizontal dipole (SCB, SCB or HDC) vertical dipole (VDC), skew-quadrupole (SKQ) and three part anti-solenoid (ASI-3) windings. The magnetic lengths and field strengths are determined by BEPC-II optics requirements for two operation modes. The first is collider mode where the SCB coil is run at low field as an closed orbit corrector (denoted HDC) and the anti-solenoid coils, ASI-3, are energized to locally compensate the effect of the BES-III detector solenoid on circulating beams. The second mode is synchrotron radiation operation for which SCB is run at its full field and the anti-solenoid coils ASI-3 are turned off (since BES-III solenoid is also off).

As described in the previous section conductor placement in the coil ends is adjusted to give proper harmonic behavior for both coil ends in order to meet the integral harmonic requirements. The three anti-solenoid coils are laid out to provide for complex field profile that is matched to the anticipated BES-III detector design and as such it is irrelevant consider their magnetic lengths separately.

The superconducting coil pack starts on the support tube with the main superconducting quadrupole, SCQ. SCQ will be built up and warm tested for harmonic content before the first and third anti-solenoid coils, AS1 and AS3 are wound. The next layers to be wound are: the main superconducting dipole, SCB (also used as superconducting horizontal bending corrector HDC), the vertically bending superconducting dipole corrector VDC, the skew-quadrupole corrector, SKQ, and finally the second anti-solenoid coil, AS2.

In order to leave space for a third anti-solenoid winding the SCQ magnetic length was shortened to 400 mm, with an associated rise in gradient to 18.744 T/m. This change

Table 3.1: BEPC-II Superconducting Magnet Coil Parameter Summary

	B, G (T), (T/m)	R _{in} , R _{out} (mm)	Distance From IP (mm)	Coil Length (mm)	Magnetic Length (mm)	Nominal Operating Current (A)
SCQ	18.744	95.1 ~ 108.1	961 ~ 1457	496	400	460
SCB (HDC)	0.543 0.056	108.5 ~ 111.8	633 ~ 1307	674	400	495 50
VDC	0.059	111.9 ~ 113.5	904 ~ 1514	610	380	20
SKQ	0.937	113.6 ~ 115.2	954 ~ 1464	510	400	45
AS1	-	91.1 ~ 105.9	630 ~ 993	303	-	1120*
AS2	-	115.4 ~ 119.0	1035 ~ 1381	346	-	1120*
AS3	-	95.1 ~ 105.9	1474 ~ 1590	116	-	1120*

*AS1-3 coils are operated in series with an option of using small trim currents for fine adjustment.

Table 3.2: Coil Winding Layout Table

Name	Number of Layers	Conductor
SCQ	8	7 Strand cable
SCB (HDC)	2	7 Strand cable
VDC	2	Single strand wire
SKQ	2	Single strand wire
AS1	6	Rectangular Wire
AS2	2	Rectangular Wire
AS3	6	Rectangular Wire

necessitates an increase in operating current and raises quench protection concerns. After an analysis was performed (see Appendix 1), we determined that SCQ should be wound as a four double-layer coil in order to have an acceptable maximum temperature rise during a quench.

As previously described, the harmonic content of the next SCQ double-layer will be adjusted to compensate undesirable harmonics. For the four-double layer SCQ coil we have three opportunities for such adjustments during production and expect to keep the final harmonics within the stated SCQ integral harmonic goal of $|B_n/B_2| < 3 \times 10^{-4}$ (@ $r = 50$ mm)

Once the SCQ coil is wound the AS1 and AS3 anti-solenoid subcoils on either side of SCQ can be laid down using rectangular cross section, MRI type, superconducting wire. The anti-solenoid coil layout inside the BES-III detector is shown in Figure 3.2 with operational requirements addressed later in Section 4. The middle anti-solenoid coil, AS2 connects between AS1 and AS3 and is the last coil to be wound on the cold mass. For the anti-solenoid the rectangular wire packs better than a circular cable would allowing a conductor with a greater copper to superconductor ratio to be used without taking up

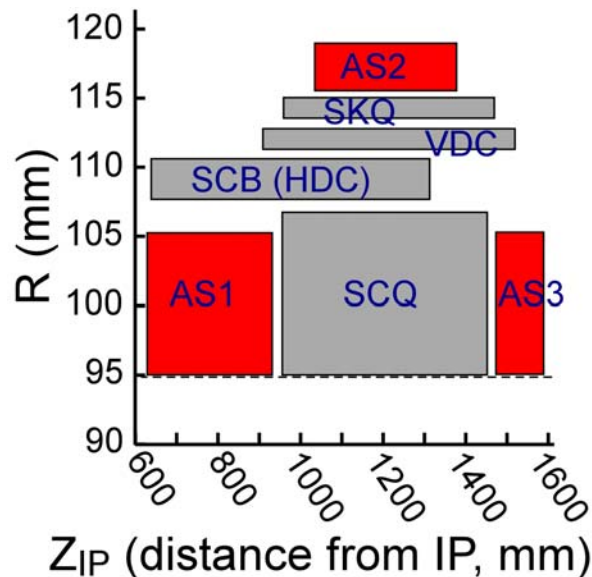


Figure 3.1. Coil Layout Schematic. Coil dimensions, conductor type and number of layers are given in Tables 3.1 and 3.2.

1/2 BES-III Detector with Anti-Solenoid

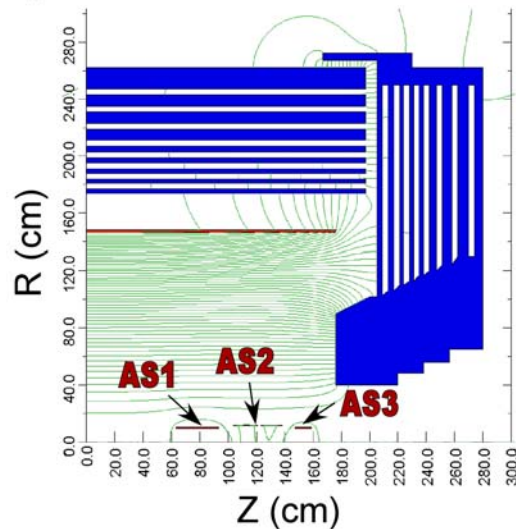


Figure 3.2: Three anti-solenoid subcoils, AS1-3 inside BES-III experimental detector. The anti-solenoid locally compensates BES-III detector field for the circulating beams. The anti-solenoid scheme is mirror symmetric about the vertical plane $Z = 0$ and rotationally symmetric about the Z -axis.

excessive radial space. The 6.88:1 Cu:Sc ratio of the MRI conductor gives additional quench protection safety for the AS1-3 anti-solenoid coils, which having more than 1,200 turns, have a large inductance.

The six winding layers used for both AS1 and AS3 give a radial buildup, as seen in Table 3.1, slightly less than that of SCQ. Thus after AS1 and AS3 are completed the AS1 region will be build up to match the SCQ outer radius in order to facilitate winding the next coil layers, the SCB dipole winding. Care is taken in the AS1 and SCB coil design to respect the requested outer cryostat (and therefore inner coil/cold mass) taper on the IP side of the magnet.

Like SCQ, the SCB coil will be wound as a double-layer coil from 6-around-1 seven strand superconducting cable. Note that, as will be elaborated in more detail in Section 4, the SCB coil requirements are driven mainly by BEPC-II synchrotron radiation operation mode; however, SCB serves double duty in collider mode as a horizontal orbit corrector denoted HDC. In synchrotron radiation operation mode the background field due to the BES-III solenoid and anti-solenoid are off and a single double-layer coil suffices to meet operational requirements. In collider mode these background fields are present, however, in this case the HDC operating current is much lower yielding more than sufficient operating margin even in the presence of solenoidal background fields. In point of fact, as will be elaborated further below, the HDC operating current must be limited at the power supply. This requirement is not set by operating current margin but rather stems from the need to limit torques experienced by the cold mass that must be passed on through the cryostat to the support assemblies. This requirement, that SCB (i.e. HDC) is never energized to its full operating current when the BES-III detector solenoid can be turned on,

is discussed further in Section 5.

It should be noted that for a dipole coil like SCB more space is needed at the coil ends to achieve proper integral harmonic compensation than required for a quadrupole coil like SCQ. Thus even though SCB and SCQ are intended to have the same magnetic length, 400 mm, the physical SCB coil length (see Table 3.1) is 178 mm longer than that for SCQ. In order to limit the magnitude of the closed orbit offset when SCB is used in synchrotron radiation mode the SCB coil is started as close to the IP as possible which however means that when this coil is used as the HDC corrector in collider mode its magnetic center is longitudinally offset from that of SCB.

Note also that since SCB consists of a single double-layer winding there is no opportunity to make field harmonic corrections in later layers. The field harmonic content expected for SCB will be worse than that can be achieved for the multilayer SCQ. Before winding SCB the coil structure will be built up atop AS1 and SCQ to be a once again uniform radius cylinder. Based upon experience gained winding the HERA-II Luminosity Upgrade magnets and an anticipated learning curve during SCQ winding we still expect to be able to meet the SCB field harmonic goal of $|B_n/B_1| < 5 \times 10^{-4}$ (@ $r=38\text{mm}$); however, it should be understood that the only recourse during production if the as wound SCB coil harmonics exceed this value is to strip off the SCB coil wiring before curing and then winding a new coil (with production and schedule impacts).

After SCB winding is finished the vertically bending corrector, VDC, and skew-quadrupole corrector, SKQ, are each wound using double-layers of single strand superconducting “corrector” wire. The corrector wire adds less to the cold mass radial buildup than coils wound from the seven-strand cable. Also the corrector wire turn spacing is about 2.3 times finer than that from cable for a correspondingly lower operating current. Since the VDC and SKQ windings are both single double-layer windings, as with SCB there is no later opportunity for harmonic correction with later coil layers. Fortunately being correctors their harmonic content goals, $|B_n/B_{1,2}| < 1 \times 10^{-3}$ (@ $r=50\text{mm}$), are relatively modest.

4. Collider and Synchrotron Radiation Mode Design Considerations

For the purposes of this discussion the main distinction between collider and synchrotron radiation operations modes for the superconducting coils is that in collider mode:

- The BES-III detector solenoid is turned on.
- The anti-solenoid coils are energized to give the on axis locally-compensated field profile shown in Figure 3.3.
- The SCB is only run at low current mode as an orbit corrector.

In synchrotron radiation operation mode:

- The BES-III detector solenoid is turned off.
- The anti-solenoid coils are turned off.
- The SCB is run at its full operational field.

The difference between these modes has significant coil design and operational consequences.

The local anti-solenoid compensation result shown in Figure 4.1 was reached by iterating on the relative number of turns in each of three anti-solenoid subcoils modeled in a finite element (Vector Fields code, Opera2d) of the projected BES-III detector solenoid that was provided to BNL by IHEP. The idea is to arrange for the AS1 coil to balance the integral longitudinal field from the IP up to the start of SCQ, AS2 to approximately null

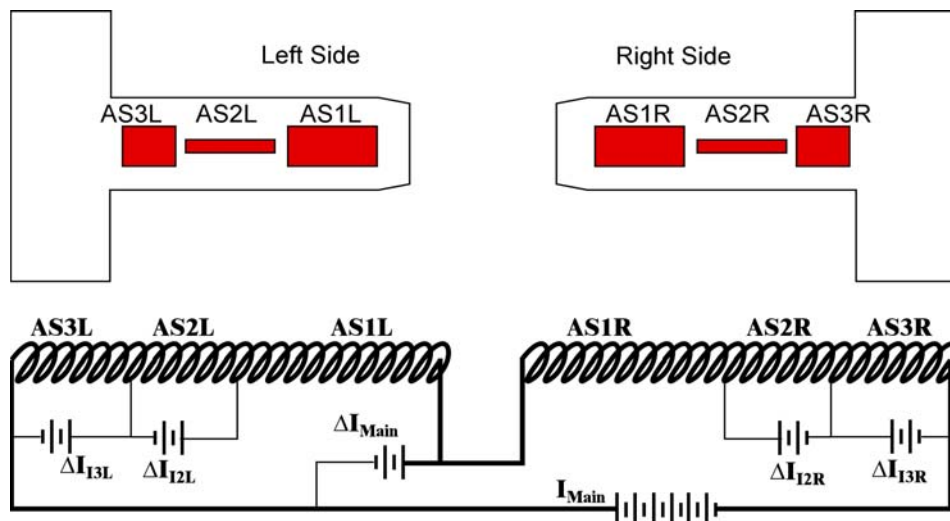


Figure 4.2: Anti-Solenoid Power Schematic. Main current of about 1120 A flows in series through all of the anti-solenoid coils. A small left-right asymmetry and small adjustments to the local compensation may be undertaken if additional trim current power supplies are provided but at the cost of additional current leads. Note that since the left and right cryostats are not directly connected independent current leads are needed on the IR right and left sides.

the field over the active length of SCQ and finally for AS3 to balance the integral field in the fringe region beyond where the cold mass ends. The solution shown in Figure 4.1 assumes that the AS1-3 coils are connected in series and have the same common excitation current running through them.

Were this compensation to be done perfectly well there would be no need to energize the skew-quadrupole coil, beyond correcting for any unanticipated SCQ roll angle, in order to correct for circulating beam coupling due to the BES-III detector. But in practice it is difficult to accurately project at this time what the final, as built, BES-III detector field configuration will be since this depends on:

- details of the BES-III detector which may change with time,
- unknown material composition details of BES-III magnetic yoke,
- and influence of the first IR separator magnets on the BES-III fringe field.

In response to the IHEP desire to avoid having to make two independent high-current, i.e. greater than 1000 A, high-cost power supplies for powering the anti-solenoid circuits on the IR right and left sides. The anti-solenoid power schematic shown in Figure 4.2 is one attempt to meet these challenges.

We have a main excitation current flowing in series throughout each of the anti-solenoid subcoils on both the right and left sides of the IR. The right-left connection is made via external copper buss work that bypasses outside the BES-III detector (i.e. assume no superconducting connection between cryostats so independent sets of current leads are needed on right and left sides). Adjustment for a small left-right asymmetry can be accommodated by adding a small shunt power supply across the main current leads on one side.

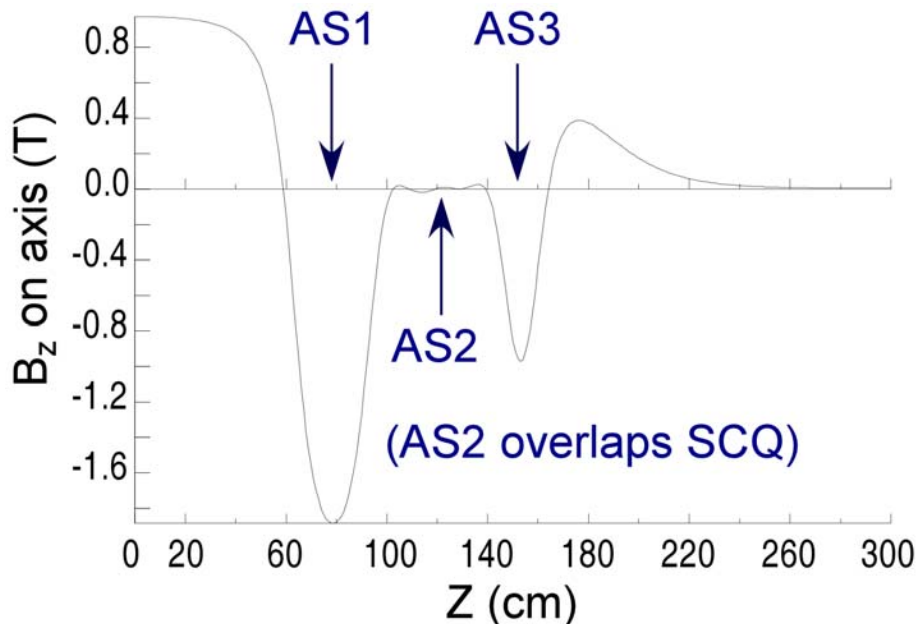


Figure 4.1: On Axis Local Compensation of BES-III Detector Solenoid Via a Three Part Anti-Solenoid.

Some flexibility for making fine adjustments to the local anti-solenoid field profile can readily be provided by bringing independent leads back to the wiring box in the endcan volume from each subcoil where the leads can be connected together and appropriate taps made. Additional trim current power supplies connected across these lead taps would permit changing the relative number of amp-turns in the subcoils. Fully implementing this scheme does bring additional power supply and quench protection consequences as outlined in Appendix 2.

5. Cold Mass Forces and Torques Due to the BES-III Solenoid

When the BES-III detector solenoid is energized the various coil windings in the cold mass experience additional forces and torques as:

- For the anti-solenoid coils the radial component, B_R , interacts with the mainly azimuthal current distribution flowing in the anti-solenoid to produce a net longitudinal force.
- For the horizontally bending dipole, HDC (SCB), the BES-III longitudinal field component, B_Z , interacts with the coil ends to produce equal but opposite vertical forces at the coil ends resulting in no net force but rather a net torque about the magnet center in a vertical plane.
- For the vertically bending dipole VDC there is again no net force but a torque acting in the horizontal plane.
- The forces acting on the coil ends will tend to drive the support tube out of round but due to quadrupole symmetry there is no net torque for either SCQ or SKQ.

Because B_R reverses direction on opposite sides of the BES-III detector, the longitudinal force acting on the right and left anti-solenoid coils are in opposite directions as indicated in Figure 5.1. In each case the longitudinal force acts so as to try to expel the anti-solenoid from the detector. We note here that since the planned attachment point on the bottom of the endcan for the support structure (see Figure 5.1) is not inline with the longitudinal force there is a net torque at the support point that has to be properly

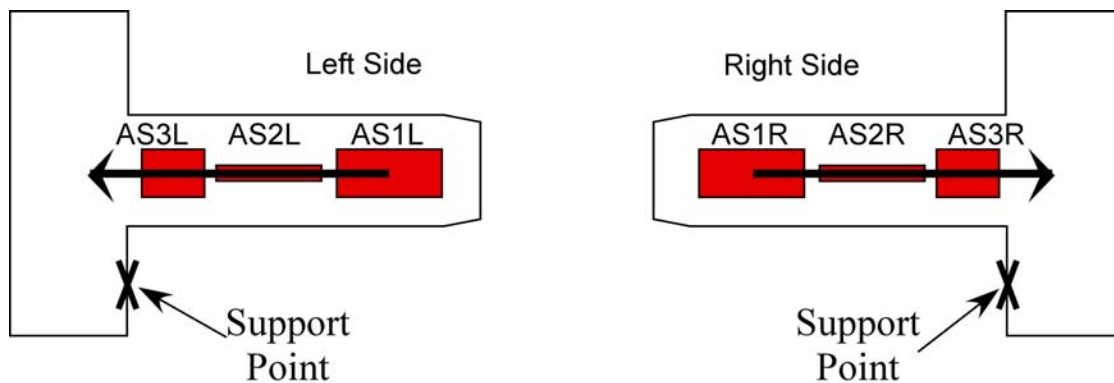


Figure 5.1: Anti-Solenoid Longitudinal Force Diagram. *Net Longitudinal force on right and left sides is equal in magnitude and opposite in direction since current flows with the same handedness on right/left sides but the BES-III radial field reverses on right and left sides.*

countered in order that the transverse centering of the magnet axis not shift with respect to the closed orbit.

The longitudinal force density distribution in the anti-solenoid coil windings in the BES-III detector, as calculated with the Opera2d code, is shown in Figure 5.2. Here the vertical axis is Z , the distance from the IP in cm, radius R in cm goes along the horizontal

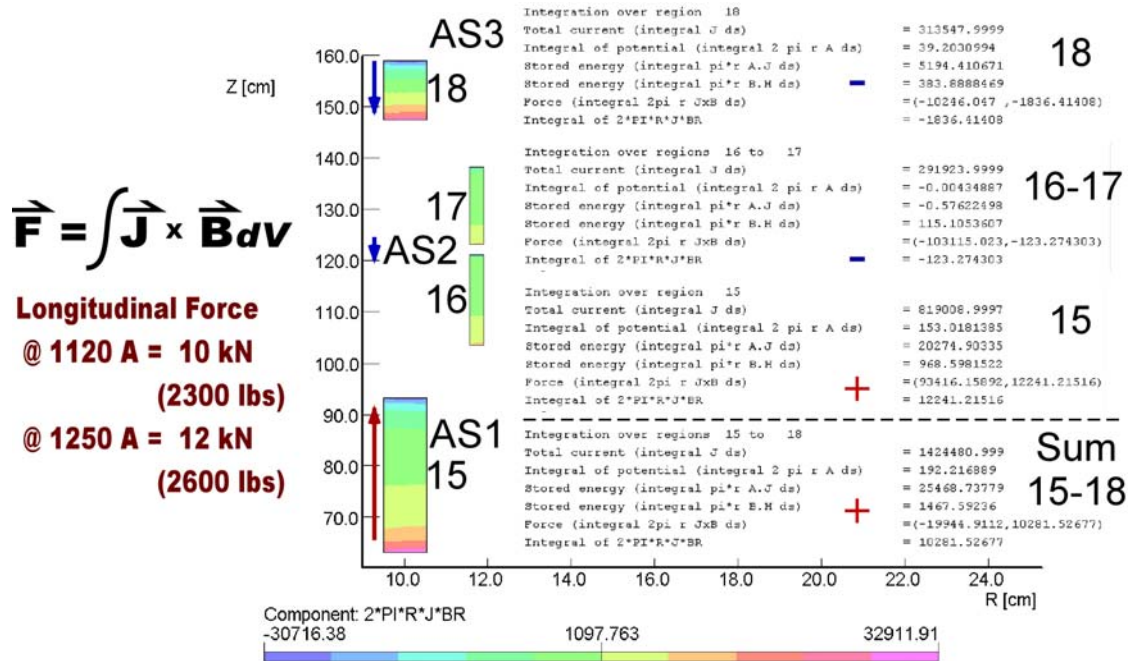


Figure 5.2: Anti-Solenoid Longitudinal Force Calculation.

axis, and the color contours correspond to the azimuthally integrated component of $\mathbf{J} \times \mathbf{B}$ in the coil (red is positive i.e. away from IP and blue negative or toward IP).

We see that AS2 and AS3, Opera regions 16-18, experience a weak inward pull since interaction between the anti-solenoid subcoils tends to try to pull them together to their common center; however, this is more than offset by the strong repulsion experienced by the AS1 subcoil, region 15. The sum for all three anti-solenoid coils yields a total longitudinal force of 10 kN (2300 lbs) with BES-III run at 1 T and the anti-solenoid is energized at its nominal operating current of 1120 A and a maximum force of 12 kN (2600) when run at a maximum current of 1250 A.

We note here that with a previous version of the anti-solenoid design, before the present AS1-3 subcoil scheme came to be adopted, had coils wound at slightly larger average radius. B_z compensation with these larger coils required a greater number of amp-turns to be used and this resulted in a somewhat higher force upper estimate of 13 kN

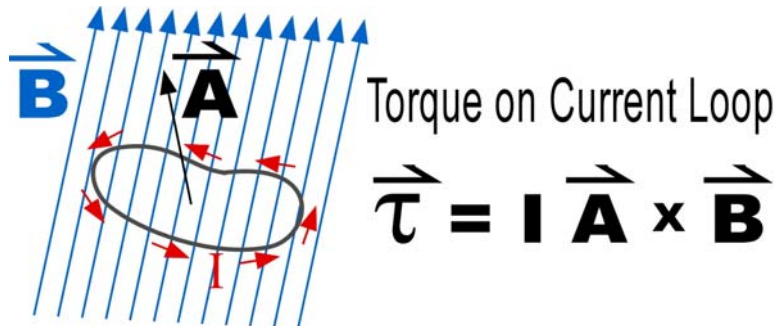


Figure 5.3: Convention for Calculating Torque for a Current Loop Embedded in a Uniform Magnetic Field.

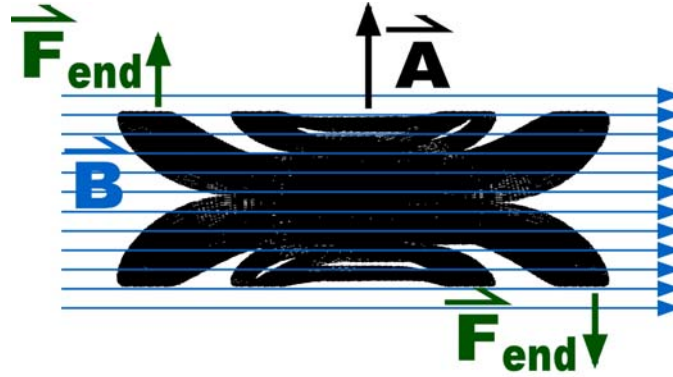


Figure 5.4: Force Diagram for a Horizontally Bending Dipole Coil Embedded in a Uniform Longitudinal Magnetic Field.

which is used for the stress calculations reported in Section 9.

The conventions used for calculating the torques on the HDC and VDC dipoles when they are energized inside the BES-III are shown in Figure 5.3, with **A** being the net coil area vector carrying current I embedded in a background field **B**.

For the case of HDC, **B** is the 1 T longitudinal field from the BES-III detector and summing over all the coil winding projects a total area of 26.6 m^2 on the horizontal plane. This yields a HDC vertical torque of 1330. Nm (980. ft-lbs) for the nominal operating current of 50 A and 1730. Nm (1280. ft-lbs) at 65 A maximum current. For VDC, **B** is still 1 T but since VDC is wound with a tighter (about 2.3 time tighter) turn spacing the total coil area is larger, 59.5 m^2 , projected on the vertical plane. Thus VDC yields a vertical torque of 1430. Nm (1050. ft-lbs) for the nominal operating current of 24 A and 3870. Nm (2850. ft-lbs) at 65 A maximum current. With HDC and VDC both energized at 65 A we can then add these torques in quadrature to determine the maximum torque 4240 Nm (3130. ft-lbs) expected for the cold mass.

It is important to understand that turning the anti-solenoid on or off does not change this cold mass torque¹. That is to say the cold mass torque has been calculated in the most convenient way, as actual forces and torques experienced by the dipole coils in a solenoidal background field with the anti-solenoid turned off; however, the cold mass will still experience the same torque with the anti-solenoid turned on (it is just more complicated to calculate).

¹To see this consider the following thought experiment. Let us assume that we have a perfect anti-solenoid that completely cancels the detector field over the volume of the dipole coil. Then with the anti-solenoid on the dipole conductors experience no net solenoidal field and are torque neutral; however, the anti-solenoid does see the external field of the dipole and therefore it now experiences its own torque due to this interaction. For a perfect anti-solenoid this torque is precisely opposite to the torque experienced by the BES-III detector due to the dipole fringe field. The net result of turning the anti-solenoid on is to shift the torque from the dipole to the anti-solenoid itself. But since the dipole and anti-solenoid are both tightly bound to the same support tube the torque experienced by the cold mass, which has to be passed to the outside world via the cryostat structure, has not been changed.

The presence of these torques has important operational consequences for BEPC-II that must be considered. The first is that unlike the constant longitudinal force experienced by the anti-solenoid when it is energized in collider mode and the BES-III solenoid is on, these dipole torques can change with time during a store as the dipole corrector currents are changed to do closed orbit steering. To be specific changing current in HDC to modify the horizontal orbit results in changing the vertical torque. But unless the support structure attached to the cryostat is very stiff this will cause the SCQ quadrupole center to change vertically resulting in an added vertical kick being given to the beam. While this is not strictly a true orbit coupling this effect, having the orbit change in both planes when beam steering is attempted, might prove troublesome for standard closed orbit adjustment algorithms. Therefore we recommend that the proposed support structure attached to the cryostat via the endcan be evaluated for motion with the maximum torque estimated above applied in an arbitrary direction.

The second area for concern is to insure that HDC is never allowed to go to the maximum 550 A maximum current, i.e. the value when used as SCB in synchrotron radiation mode, with the BES-III detector energized. In going from 65 A to 550 A excitation the cold mass torque rises from 3,870 Nm to 14,600 Nm (10,800 ft·lbs) which is beyond the level permitted for the cryostat support structure. To be able to handle such a large torque the support keys (i.e. G10 and stainless steel pieces) would have had to be strengthened and this in turn would lead to an even higher heat load at 4°K than those calculated in Section 8 of this report. In order to minimize the heat load seen by the cryogenic system such strengthening was not done.

Thus an interlock procedure is needed to ensure that during BEPC-II collider mode when the BES-III detector is energized the HDC and VDC currents are not allowed to go beyond 65 A and during BEPC-II synchrotron radiation mode, where SCB (HDC) is allowed to go to 550 A, that the BES-III solenoid cannot be accidentally turned on.

6. Overview of Mechanical Design

A 3-D model of the assembled magnet has been developed. The model is bounded by the vacuum enclosure at the IP end, and the helium end box inside a vacuum end volume at the non-IP end. The non-IP end is the end where the magnet coil power leads and instrumentation leads exit, through a port in the face of the end volume which also serves as the 4K helium supply line. A 4K helium return line and heat shield helium lines also exit through the same port. The model begins radially with an inner vacuum vessel. Working outward, a series of concentric tubes serve as inner heat shield, inner helium vessel, coil support tube, outer helium vessel, outer heat shield, and outer vacuum vessel. The helium flow is provided both to the inner radius of the coil support tube and the outer radius of the coils for effective cooling. The conductive heat load on the magnet coils is minimized by the use of thin stainless steel support keys, aligned with and welded to the outer vacuum vessel. These keys engage slots in NEMA grade G-10 retainers, arranged in a 90° pattern around the circumference of the outer helium vessel, in two axial locations. Besides being optimized for minimum heat flux, while retaining structural integrity, these G-10 retainers are also mechanically heat stationed to the 80K heat shield. In addition to these sliding supports, the coil assembly is supported axially by a separate Ultem thermoplastic polyetherimide support at the magnet lead end. All supports have been optimized to minimize heat load while being able to withstand the magnetic Lorentz forces, and are described in greater detail below.

From the 3-D mechanical model, a preliminary assembly drawing of the magnet has been created and is included as an electronic file on compact disc. Also, detailed drawings of the individual parts needed to build the magnet have been created, and are included in preliminary form on the disc as well. A full listing of the assembly drawing number and drawing numbers of the detailed parts drawings is included in Appendix 3.

A review of the various components for pressure vessel safety has been started. For this purpose, consistent with other international programs completed previously, BNL has used the ASME Pressure Vessel Code as a guide for determining pressure vessel safety. These calculations are provided for review in Section 7. Also included is a description of pressure vessel safety tests to be completed.

Analyses of the mechanical stresses and heat flows through the magnet supports have been completed using Mechanica® and Pro/Engineer® software from PTC Inc. The focus of the analyses has been to optimize the support system, minimizing the heat load as possible while maintaining the mechanical stresses caused by the magnetic Lorentz forces to be within acceptable limits for the thermoplastic supports. Results are shown in Section 9.

7. Pressure Vessel and Safety Certification

- I. A.S.M.E. Code
- II. Calculations
 - A) Inner Cryostat Vessel
 - B) Inner Helium Vessel
 - C) Helium Outer Vessel
 - D) Outer Cryostat Vessel
 - E) Cryostat End Volume Housing
 - F) Lead Box
 - 1) bottom flange
 - 2) housing
- III. Pressure Testing

The following section contains calculations done in accordance with the A.S.M.E. (American Society of Mechanical Engineers) Pressure Vessel Code. Satisfaction of this code insures safe operation and is required for any pressure vessel to be certified for use.

Use of equations, tables and stress values from the pressure vessel code have the required safety factors already included.

Inner Cryostat Vessel (21010016)

Specifications:

Design Pressure: 15 psi (1 bar) internal

Material: 316L stainless steel

Inner Diameter: 5.276" (134mm)

Thickness: .098" (2.5mm)

Minimum required thickness from Section UG-27 determined by:

$$t = \frac{PR}{SE - .6P}$$

P = 15 psi

R = 5.276/2 = 2.638"

S = Maximum allowable stress (table UHA-23) 316L welded seam tube

= 16,000 psi (110 mpa)

E = weld joint efficiency since seam weld is already factored into maximum allowable stress (E = 1.0)

$$t = \frac{15 \text{ psi}(2.638")}{16,000 \text{ psi} - .6(15)} = \frac{39.57}{15,991}$$

$t_{\min} = .003"$, significantly less than design and therefore acceptable.

Inner Helium Vessel (21010017)

Specifications:

Outer diameter:	6.840" (173.74mm)
Thickness:	.187" (4.75mm)
Length:	43.045" (1093.35mm)
Material:	316L stainless steel
Design Pressure:	295 psi (20 bars) external

From Section UG-28, allowable pressure determined by:

$$\frac{D_0}{t} = \frac{6.840}{.187} = 36.6$$

$$\frac{L}{D_0} = \frac{43.045}{6.840} = 6.3$$

A factor from chart (5-UGO-28.0)

$$A = .00095$$

From chart 5-UHA-28.4

$$B \text{ Factor} = 9,200 \text{ psi}$$

$$P_{\text{allowable}} = \frac{4(B)}{3(D_0/t)} = \frac{4(9200)}{3(36.6)} = 335 \text{ psi (22.8 bars)}$$

335 is greater than 295 so vessel exceeds minimum requirements

Helium Outer Vessel (21010020)

Specifications:

Design pressure:	295 psi (20 bars) internal
Material:	316L stainless steel
Inner diameter:	9.37" (238mm)
Thickness (t):	.138" (3.5mm)

Minimum required thickness for internal pressure from section UG-27 is determined by

$$t = \frac{PR}{SE - .6P}$$

$$P = 295 \text{ psi}$$

$$R = 9.37"/2 = 4.685"$$

S = Maximum allowable stress (from Table UHA-23) for 316L welded STN.STL tube

$$\begin{aligned} \text{Spec \#SA-249} \\ = 16,000 \text{ psi (110 mpa)} \end{aligned}$$

E = Weld joint efficiency

Since seam weld is already factored into the maximum allowable stress (s), E = 1.0

$$t = \frac{295(4.685)}{16,000(1.0) - .6(295)}$$

$$t = \frac{1382.1 \text{ lbs/in}}{15823 \text{ lbs/in}^2} = .087"$$

required thickness is .087" (2.21mm) so 3.5mm thickness is acceptable.

Outer Cryostat Vessel (21010015)

Specifications:

Pressure (P):	15 psi (1 atm) external
Tube O.D. (D_0):	11.809" (302mm)
Thickness (t):	.236" (6mm)
Length (L):	37.54" (953.5mm)
Material:	316L stainless steel (welded seam)

From Section UG-28 allowable pressure determined by:

$$D_0/t = \frac{11.809}{.236} = 50.0$$

$$\frac{L}{D_0} = \frac{37.54}{11.809} = 3.18$$

From chart UGO-28.0

$$\text{Factor A} = .0012$$

From chart 5-UHA-28.4,

$$\text{B Factor} = 9500$$

$$\text{Allowable Pressure} = \frac{4B}{3(D_0/t)} = \frac{4(9500)}{3(50)} = 253 \text{ psi (1.75 mpa)}$$

Allowable pressure is well over the 15 psi design (P)

Cryostat End Volume Housing (21010010)

Specifications:

Design Pressure: 15 psi (1 atm) external
Material: 6061-T6 Aluminum
Outer Diameter: (23.25") 590.64mm
Length: 13" (331.6mm)
Thickness: .197" (5mm)

From Section UG-28 allowable pressure determined by:

$$\frac{D_0}{t} = \frac{23.25}{.197} = 118$$

$$\frac{L}{D_0} = \frac{13}{23.25} = .56$$

From chart 5-UGO-28

A Factor = .002

From chart 5-UNF-28.30

B Factor = 8300

$$\text{Maximum allowable } P = \frac{4B}{3(D_0/t)} = \frac{4(8300)}{3(118)} = 93.8 \text{ psi } (.65 \text{ mpa}) > 15 \text{ psi } \checkmark$$

Lead Box Bottom Flange (21010025)

Required thickness determined by:

$$t = d \sqrt{\frac{CP}{SE}}$$

where

Material =	316L stainless steel
d (Diameter) =	6.114" (155.3mm)
P (Design Pressure) =	295 psi (20 bar)
S (Max Allowable Stress) =	15,700 psi (110 mpa)
C (Attachment Factor) =	.33 (from chart UG-34)
E (Weld Efficiency) =	.65 (single butt weld with backing strip)

$$t = d \sqrt{\frac{.33(295)}{15,700(.65)}} = 6.114 \sqrt{\frac{97.35}{10,205}}$$

$$t_{\min} = .597" \text{ (required thickness)}$$

actual thickness is .625" (Acceptable).

Lead Wiring Box Housing (21010024)

Specifications:

Design Pressure: 295 psi (20 bar) Internal
Material: 316L stainless steel
Inner Diameter: 5.760" (146.3 mm)
Thickness: .120" (3.05 mm)

Required thickness from Section UG-27 determined by:

$$t = \frac{PR}{SE - .6P}$$

$$P = 295 \text{ psi}$$

$$R = 5.760/2 = 2.88''$$

$$S = 16,000 \text{ psi}$$

E = weld joint efficiency since seam weld is already factored into the maximum allowable stress E = 1.0

$$t = \frac{295(2.88)}{16,000 - .6(295)} = \frac{849.6}{15,823}$$

$$t_{\min} = .054'' (1.36 \text{ mm})$$

Required thickness is less than half of design.

Pressure Leak Testing

1. Upon completion of the cold mass assembly (4K Helium Vessel) the completed assembly will be hung vertically in a dewar. The dewar will then be evacuated below 4 millitorr. The helium vessel will then be pressurized with helium to 110% of its design value (25 bars). Pressure will be held for 10 minutes, thus satisfying the requirements for pressure vessel safety. In addition, leak detection devices will check for the presence of helium during that time. Leak rate not greater than 2×10^{-10} std.cc He/sec serves as a secondary assurance for proper magnet operation.
2. Prior to shipment, the final magnet assembly will be pressurized to 110% of its design pressure (22 bars) and helium detection will be performed.

8. Cold Mass Heat Leak Calculations at 4°K

- I) Conduction and Radiation through Multi Layer Insulation (MLI) into coldmass
 - A) From 80K shield
 - B) From 300K environment
- II) Conduction Through Key Supports
- III) Conduction Through Axial Support
- IV) Total

To estimate the total heat leak from conduction and radiation through superinsulation assuming the cold and warm surfaces are approximately equal, use equation derived by Ralph Shutt¹:

$$Q = \frac{1}{N} [1.22 \times 10^{-3} P (T_0^{1/4} - T_i^{1/4}) + 3.22 \times 10^{-14} (T_0^{17/4} - T_i^{17/4})]$$

Where Q is the heat leak in W/cm², P is the pressure in microns, and N is the number of layers of insulation.

If Q is plotted as a function of N for different pressures and T₀'s and T_i's, curves such as the following may be obtained.

By assuming what pressure may be achieved between layers of insulation, an estimate may be made of the heat leak in W/cm² as a function of number of layers.

Superinsulation:	Aluminized Mylar	0.00025 in.
	+ <u>Remay insulation</u>	+ <u>0.003 in</u>
	Layer thickness	0.00325 in ~ 0.08 mm

Assume because of compression, joints, etc., effective heat leak of super insulation is a factor 4 greater than indicated by the curves.

¹Referenced in Brookhaven National Laboratory Magnet Division Note 504-16 (RHIC-MD-208).

Conduction and Radiation From 80K

Total Area

Inner Vessel

$$\pi(16.42 \text{ cm})(109.3 \text{ cm}) = 5638 \text{ cm}^2$$

Outer Vessel

$$\pi(24.5 \text{ cm})(94.5 \text{ cm}) = 7274 \text{ cm}^2$$

Non Lead End Cap

$$\begin{aligned} \frac{\pi}{4}(21.4^2_{\text{cm}} - 17.3^2_{\text{cm}}) + (23.8^2_{\text{cm}} - 21.4^2_{\text{cm}}) \frac{\pi}{4}(1.414) + 1.1(23.8_{\text{cm}}) \pi \\ = 124.6\text{cm}^2 + 120.5 \text{ cm}^3 + 82.2 \text{ cm}^2 = 327 \text{ cm}^2 \end{aligned}$$

End cap and outer vessel will have 40 layers of MLI.

Inner vessel will have 25 layers.

From Figure 8.1 $Q_{40} = .7 \times 10^{-5} \text{ w/cm}^2$ (for 40 layers)

$$Q_{25} = .85 \times 10^{-5} \text{ w/cm}^2 \text{ (for 25 layers)}$$

$$H_{80} = (7274 + 327) \text{ cm}^2 (.7 \times 10^{-5} \text{ w/cm}^2) 4 + 5638 \text{ cm}^2 (.85 \times 10^{-5} \text{ w/cm}^2) 4$$

$$H_{80K} = .21\text{w} + .19 \text{ w}$$

$$H_{80K} = .4 \text{ w}$$

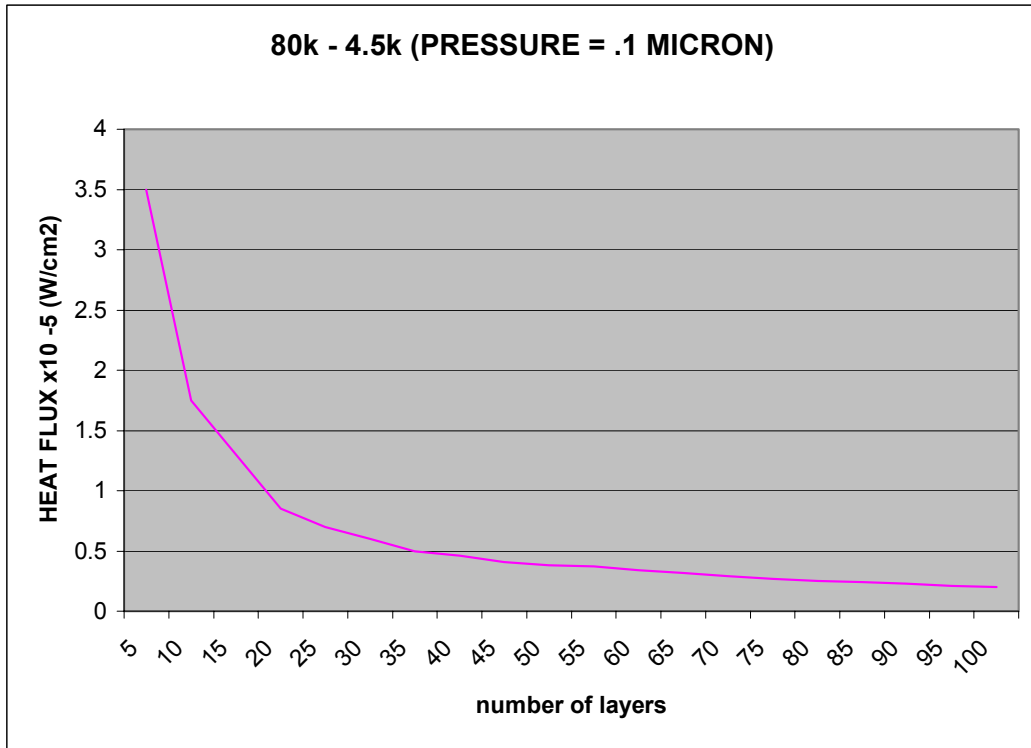


Figure 8.1

Conduction and Radiation From 300K

Area

Over outer vessel (24.5_{cm}) π 13.2 cm = 1016 cm²

Lead end cap = $(23.8^2_{\text{cm}} - 17.5^2_{\text{cm}}) \frac{\pi}{4} = 204 \text{ cm}^2$

From Figure 8.2

Q_{300} for 40 layers of MLI = $3.4 \times 10^{-5} \text{ w/cm}^2$

$H_{300} = (1016 \text{ cm}^2 + 204 \text{ cm}^2) 3.4 \times 10^{-5} \text{ w/cm}^2 (4) = .17 \text{ w}$

Total heat load from radiation and conduction through MLI

= .4w + .17 w = .57 w

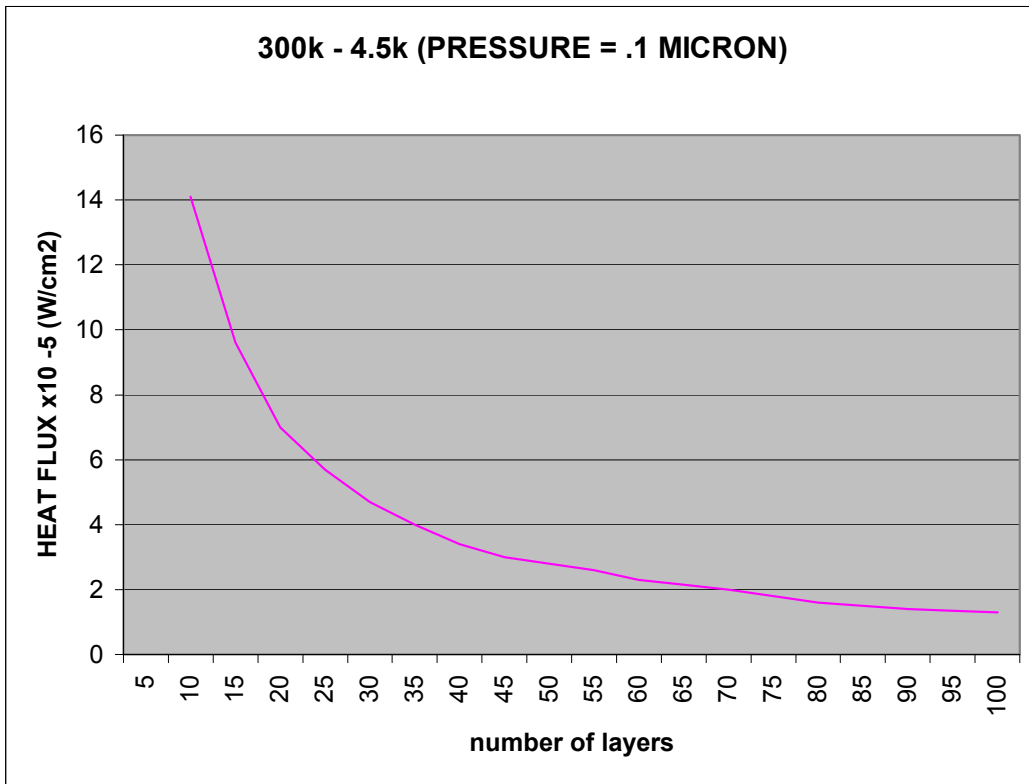


Figure 8.2

Conduction From Key Support

From finite element analysis (see Figure 8.3) average flux through key section is

$$\sim 8 \text{ mw/mm}^2$$

area through section

$$= 29.5 \text{ mm} (5.5 \text{ mm}) + (5.5 \text{ mm})^2 \frac{\pi}{4}$$

$$162.25 + 23.75 = 186 \text{ mm}^2$$

$$H = 8 \text{ mw/mm}^2 (186 \text{ mm}^2) \sim 1.5 \text{ w/key}$$

Total Heat From Keys

$$8 (1.5 \text{ w/key}) \sim 12.0 \text{ w}$$

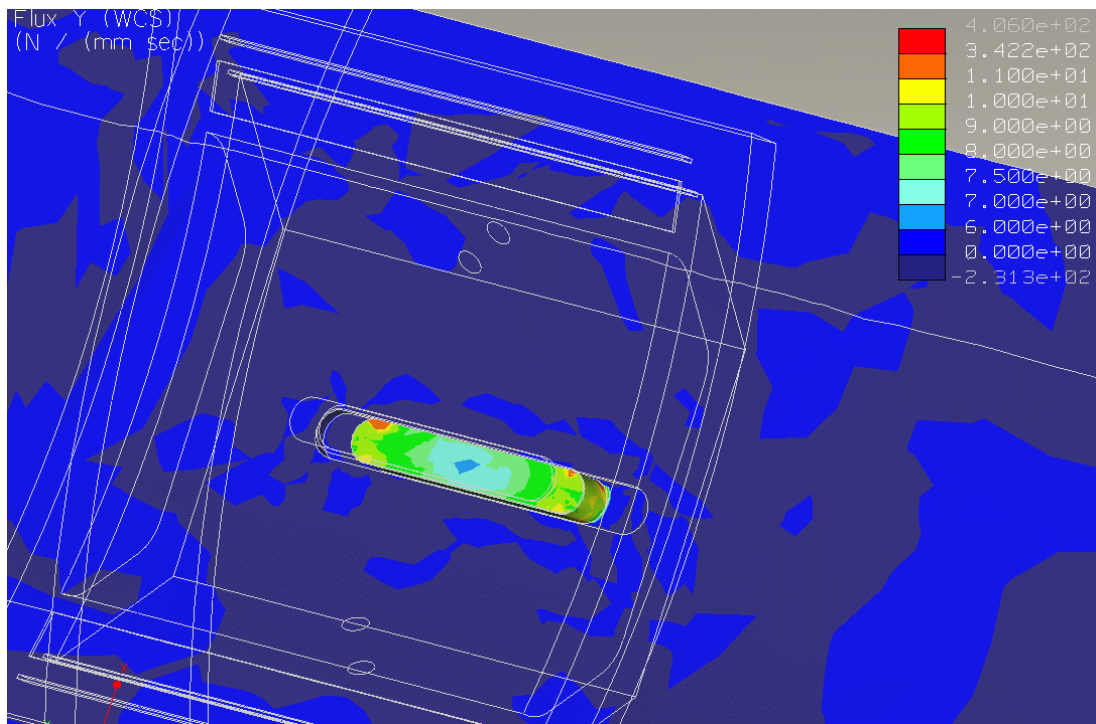


Figure 8.3 Key Flux 6-13.

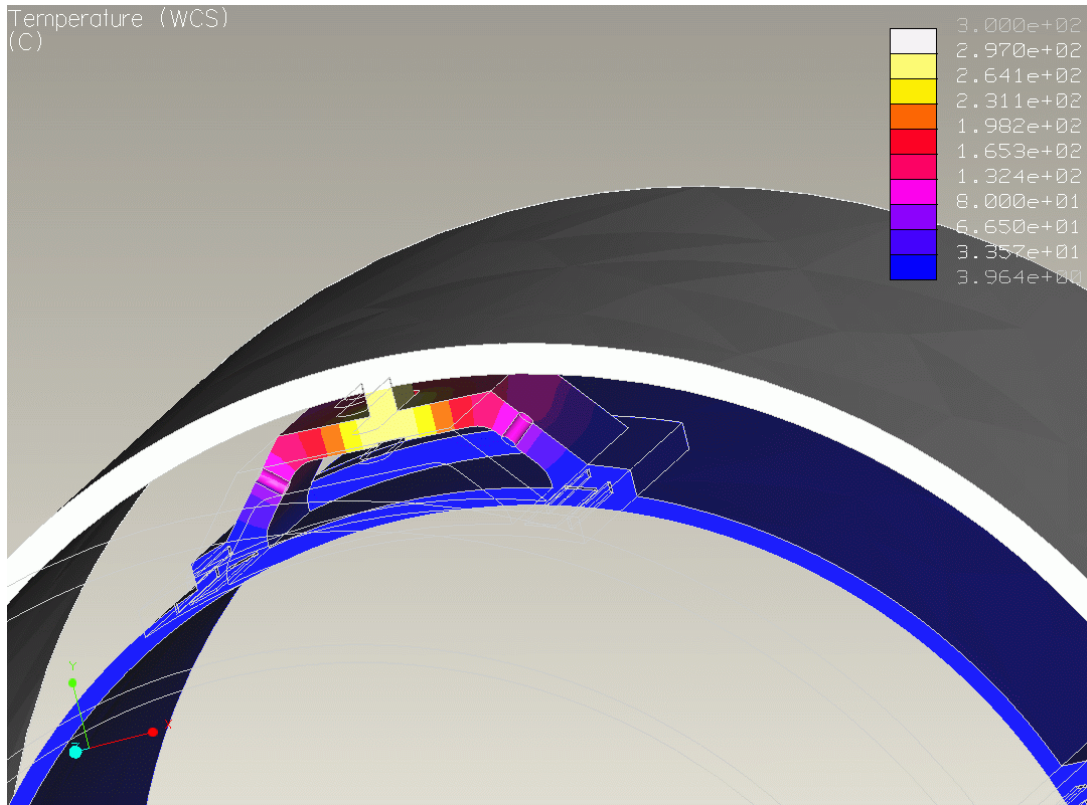


Figure 8.4 Key Temp 6-13.

Conduction Through Axial Support

- 1) From finite element analysis (see Figure 8.5)

Average heat flux through section

$$= .35 \text{ mw/mm}^2$$

- 2) Area of section through arc

$$(168_{\text{mm}}^2 - 160_{\text{mm}}^2) \frac{\pi}{2} + 30 \text{ mm} (8 \text{ mm}) = 4361 \text{ mm}^2$$

$$\text{Head load} = .35 \text{ mw/mm}^2 (4361 \text{ mm}^2) = 1526 \text{ mw} = 1.52 \text{ watts}$$

Total Heat Load to 4 K System

1)	Conduction & Radiation through MLI	=	.57w
2)	Conduction through axial support	=	1.52w
3)	Conduction through key supports	=	<u>12.0w</u>
	Total	=	14.09w

- The total estimated heat load to the 4K system is ~ 14 watts per magnet.

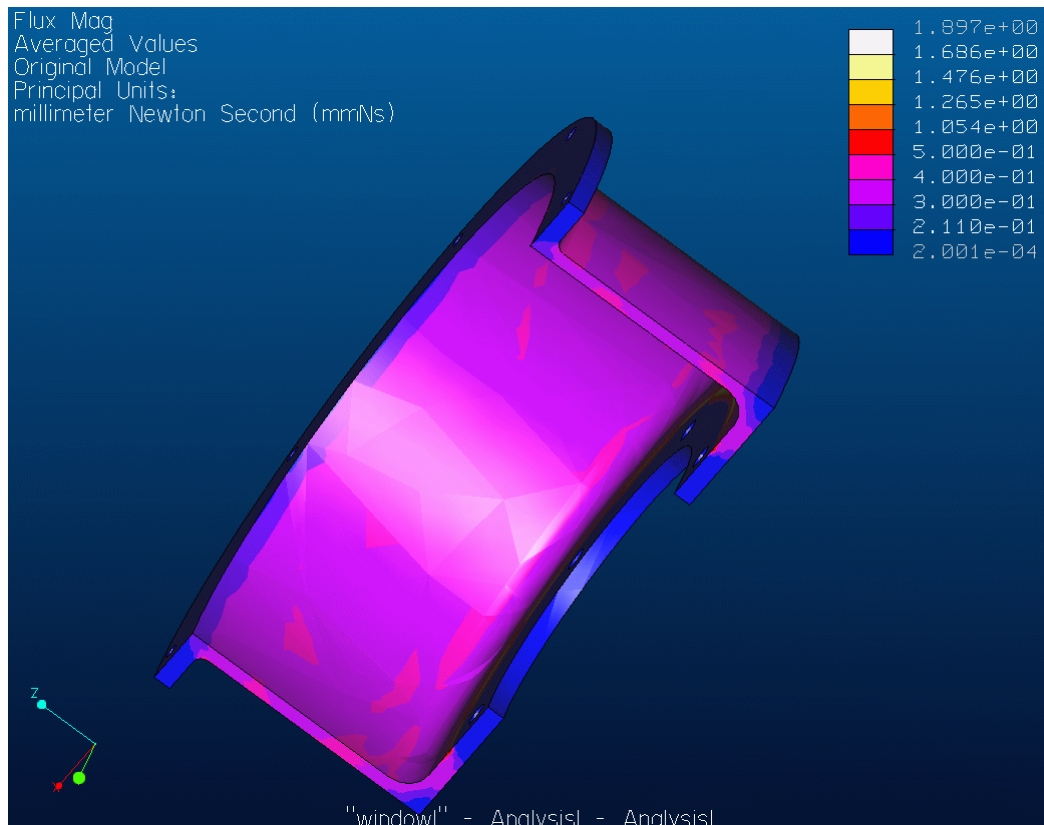


Figure 8.5 Axial Support Flux.

9. 3D Structural Analysis

Axial Restraint

Analysis of the axial restraint was done with a 13KN load applied both toward and away from the I.P. In practice the restraint should only see the load applied away from the I.P. and from the analysis we see that this load produces the highest stresses. Material is Ultem 2400 polyetherimide thermoplastic with a tensile yield stress of 190 MPA and a compressive yield stress of 220 MPA. Analysis shows a very local peak stress of 97 MPA with the average stress in the rest of the part to be 50 MPA. (See Figure 9.2) All stresses are well below the yield values with a safety factor of at least 2. Figure 9.3 shows 13 KN load applied toward I.P.

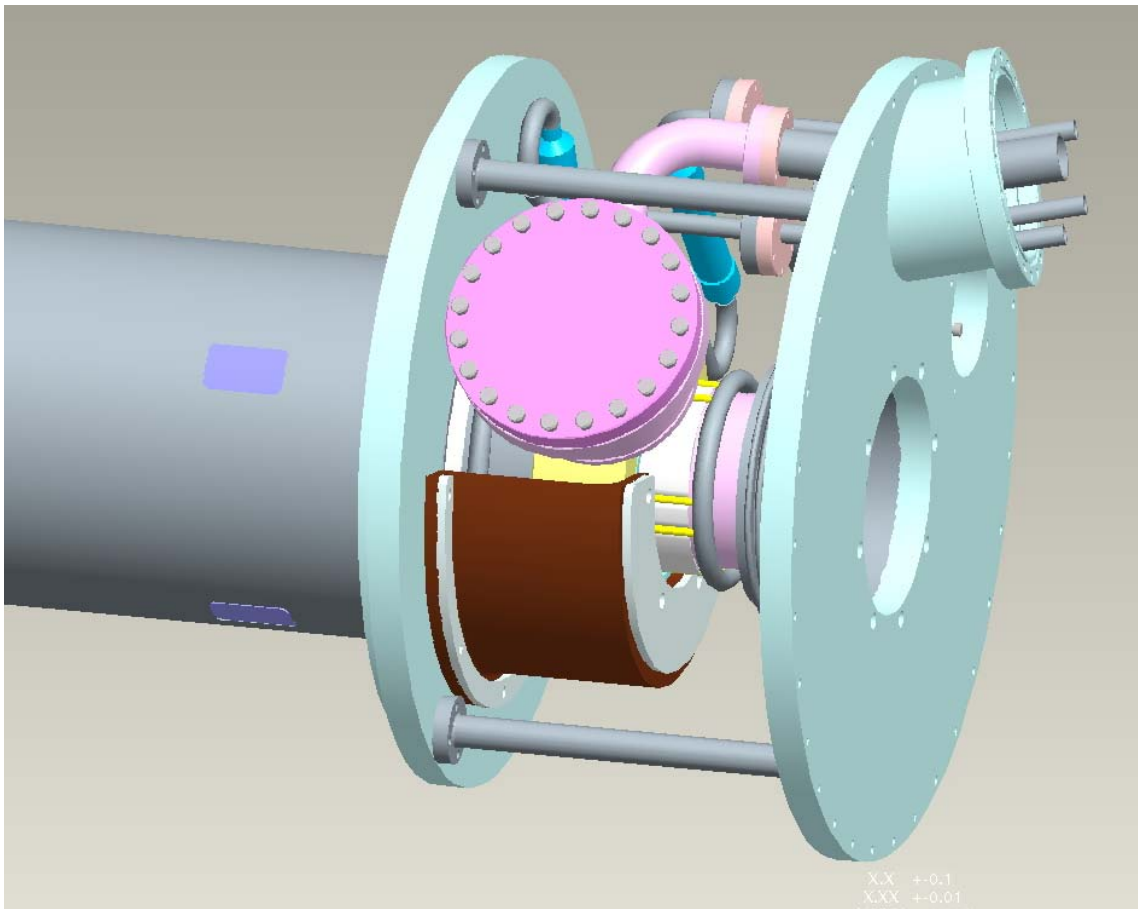


Figure 9.1: Axial Support Detail. Axial support (shown in brown) transmits longitudinal force from cold mass to endcan structure.

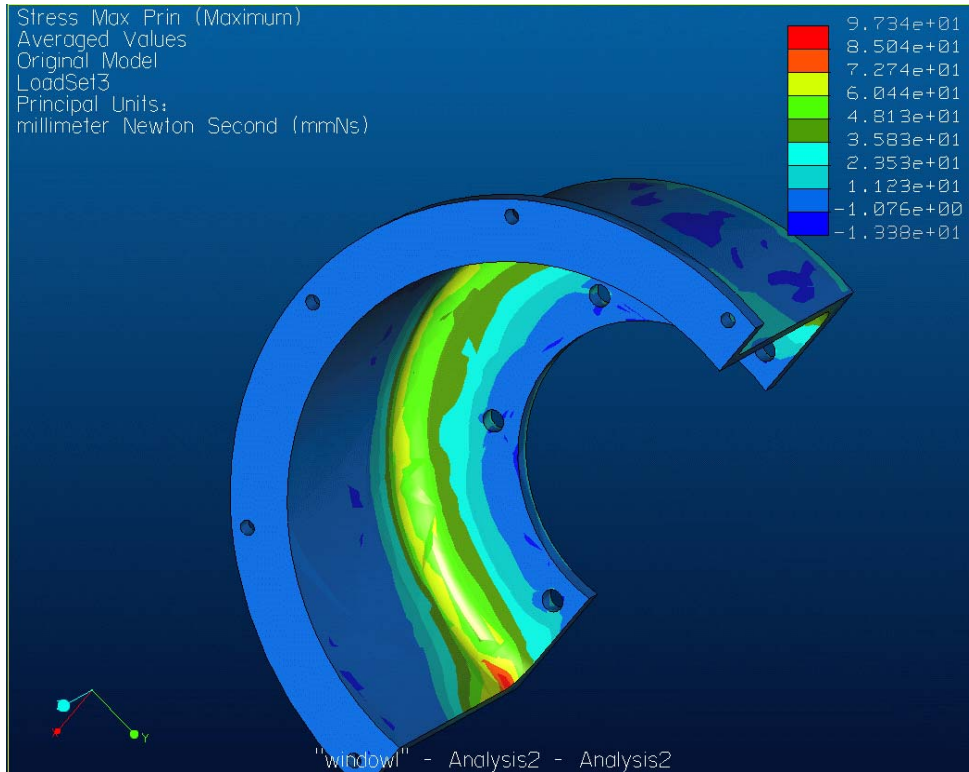


Figure 9.2: Axial Stress Outward.

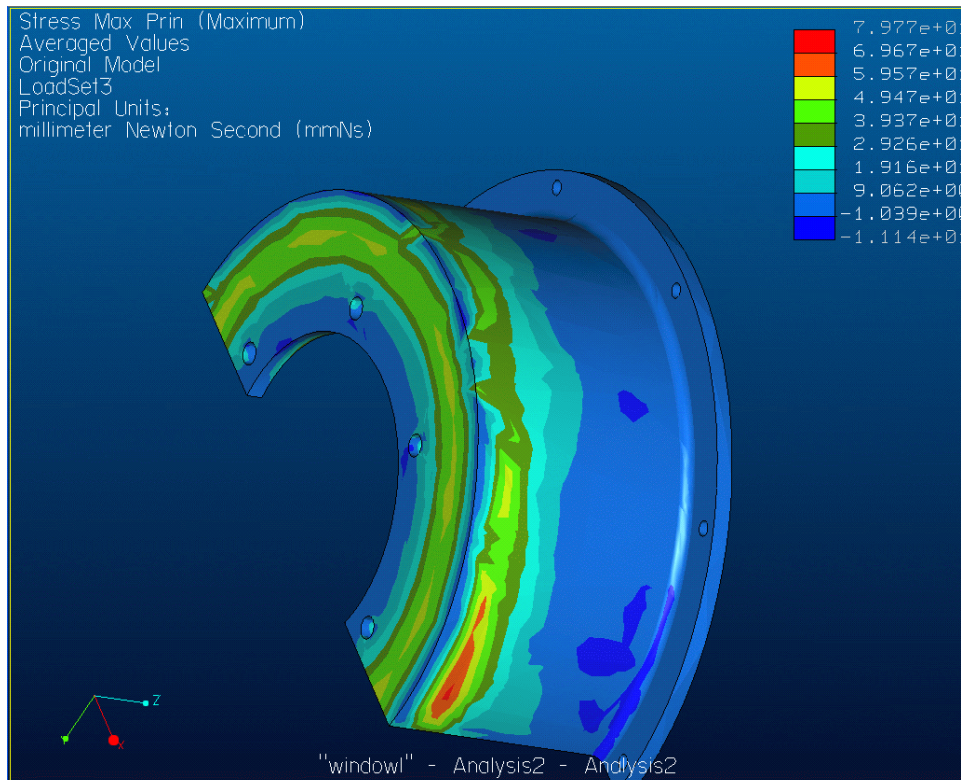


Figure 9.3: Axial Stress Inward.

Key Support Stress

An analysis on the supports was done with a 2250 N force applied to them. This should simulate the combined load from all magnetic forces. From Figure 9.4 it is seen that the stresses in the stainless steel keys are less than 70 MPa. There is a very small stress concentration in a sharp corner but this can easily be eliminated by the addition of a small radius. Stresses in the G-10 retaining pad are all below 30 MPa. It is determined from this that the stresses in both parts have a more than adequate margin of safety for use.

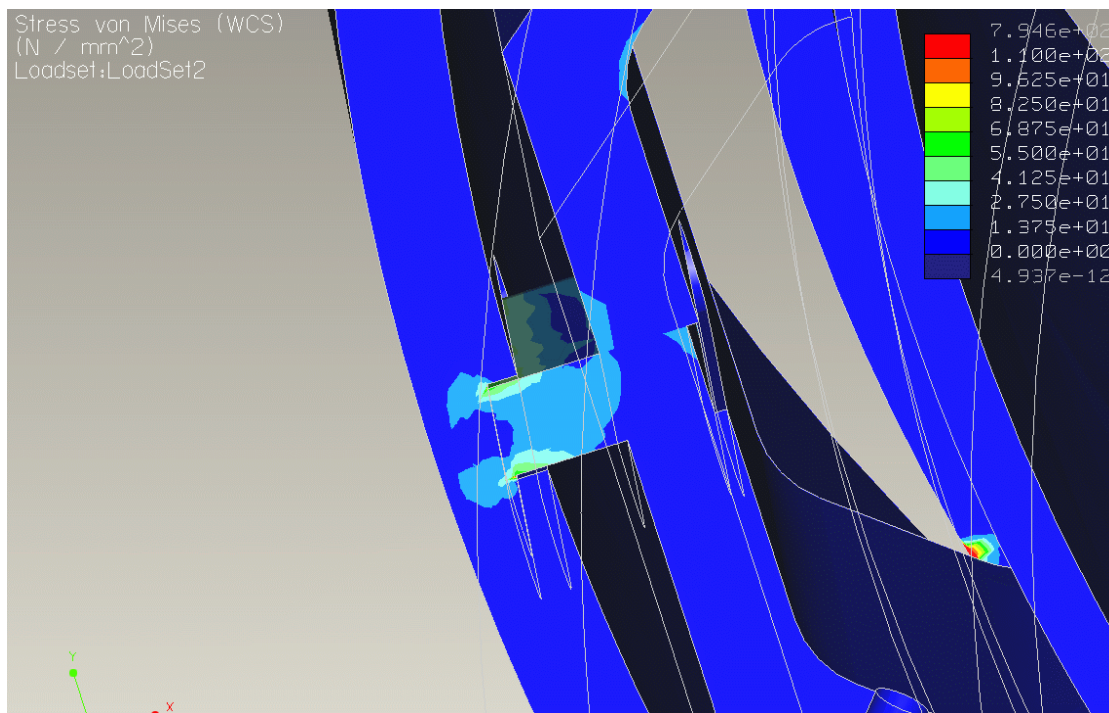


Figure 9.4: Key Stress 10006-16.

10. Magnet Interface

I. End Can Connection

- A) Access
- B) Cryogenic Connections
- C) Lead Connections

II. Cryostat Mounting

I. End Can Connection

A) Access

Access to the end can for connections to the lead tower and magnet service is done with a sliding sleeve (Housing) that slides toward the IP for access. It is a bolted connection with O-ring seals for repeated access.

B) Cryogenic Connections

All four cryogenic pipes will enter the end can through a single 154 mm diameter opening. This opening will be placed 35° counter-clockwise from the 12 o'clock position and angled vertically 10°. The four cryogenic pipes:

- 4K Helium supply
- 4K Helium return
- 80K shield supply
- 80K shield return

will enter through this opening and connect to the magnet with 2.75" (69.85 mm) conflat metal seal gaskets. The magnet pipes will contain flex hose assemblies on all pipes to allow for misalignment and differential thermal contraction, except on the 4K helium supply line, which is also the magnet coil lead box connection. It is recommended that the 152 mm transfer line jacket from the lead tower contain a bellows assembly to allow for thermal contraction.

Mating pipe stubs and flanges will be provided for attachment to the lead tower.

C) Lead Connections

Access to the lead box is also provided by the sliding sleeve. The wiring box has a bolted on cover (conflat flange and metal gasket). With cover removed the leads can then be connected from the magnet to the lead tower along with the voltage taps. The wiring box also contains (2) G-10 boards, which contain the voltage tap resistors and have provisions for securing the lead connections.

II. Cryostat Mounting

The present support proposed by IHEP for mounting the cryostat connects to the front of the front plate and surrounds the bottom half of the end can and magnet cryostat. This method of mounting will prevent the sliding sleeve from moving thus prohibiting access to the end can. It is our strong feeling at Brookhaven that this should be carefully considered as access to the magnet will then require a great deal of disassembly of support structure and possibly also require the use of temporary supports.

11. Open Issues

I. Survey Features

The magnetic field of the magnets will be referenced to external fiducials on the cryostat. Some preliminary ideas and sketches have exchanged, however the final configuration of what the survey features need to be has yet to be decided upon.

Appendix 1. SCQ Quench Protection Design Study Comparison

The maximum conductor temperature due to a quench has been estimated for four design options for the SCQ magnet. The superconductor can be made with a copper-to-superconductor ratio of either 1.8:1 or 2.5:1. (The HERA magnets used 1.8:1 superconductor; the helical magnets used 2.5:1 superconductor.) The coils can contain either three or four double layers. For each of the four options, the maximum temperature has been estimated for three currents: the operating current, 110% of the operating current, and the quench current.

The maximum temperature is determined by integrating the square of the current during the quench ($\int I^2 dt$). For this magnet, the result is conveniently expressed in units of $10^3 A^2 s$, written as KI^2dt , and pronounced “kites”. KI^2dt is used because no extra instrumentation (e.g., voltage taps) is needed for measuring it. The correspondence between KI^2dt and conductor temperature is established by adding voltage taps and a small heater (“spot heater”) to a short length of conductor. The heater is used to induce quenches in the conductor for a range of currents. The voltage taps measure the resistance of the copper in the short length of conductor. The temperature is obtained from standard tables of copper resistivity as a function of temperature. Measurements of the 1.8:1 and the 2.5:1 cables are plotted in Figures A1.1 and A1.2, respectively. As expected, the cable with the larger amount of copper can absorb more KI^2dt before reaching a given

Table A1.1: Quench Calculations for a Three Double-Layer SCQ.

Double Layers	Cu:Sc Ratio	Inductance	Initial Current	Quench R	KI^2dt	Conductor Temp.
3	1.8:1	0.15	620 (1)	X 1	41	≈ 260 ° K
3	1.8:1	0.15	620 (1)	X .5	49	≈ 400 ° K
3	1.8:1	0.15	620 (1)	X .25	61	≈ 550 ° K
3	1.8:1	0.15	685 (2)	X 1	50	≈ 400 ° K
3	1.8:1	0.15	685 (2)	X .5	59	≈ 540 ° K
3	1.8:1	0.15	685 (2)	X .25	74	≈ 750 ° K
3	1.8:1	0.15	840 (3)	X 1	74	≈ 750 ° K
3	1.8:1	0.15	840 (3)	X .5	88	> 800 ° K
3	1.8:1	0.15	840 (3)	X .25	111	> 1000 ° K
3	2.5:1	0.15	620 (1)	X 1	41	≈ 230 ° K
3	2.5:1	0.15	620 (1)	X .5	49	≈ 350 ° K
3	2.5:1	0.15	620 (1)	X .25	61	≈ 600 ° K
3	2.5:1	0.15	740 (3)	X 1	58	≈ 580 ° K
3	2.5:1	0.15	740 (3)	X .5	69	≈ 700 ° K
3	2.5:1	0.15	740 (3)	X .25	86	> 800 ° K

Notes:

1 = operating current

2 = operating current + 10 %

3 = quench current

Table A1.2: Quench Calculations for a Four Double-Layer SCQ.

Double Layers	Cu:Sc Ratio	Inductance	Initial Current	Quench R	KI^2dt	Conductor Temp.
4	1.8:1	0.26	475 (1)	X 1	27	$\approx 110^\circ \text{K}$
4	1.8:1	0.26	475 (1)	X .5	34	$\approx 180^\circ \text{K}$
4	1.8:1	0.26	475 (1)	X .25	45	$\approx 330^\circ \text{K}$
* 4	1.8:1	0.26	525 (2)	X 1	33	$\approx 170^\circ \text{K}$
* 4	1.8:1	0.26	525 (2)	X .5	41	$\approx 275^\circ \text{K}$
* 4	1.8:1	0.26	525 (2)	X .25	55	$\approx 480^\circ \text{K}$
4	1.8:1	0.26	765 (3)	X 1	71	$\approx 680^\circ \text{K}$
4	1.8:1	0.26	765 (3)	X .5	87	$> 800^\circ \text{K}$
4	1.8:1	0.26	765 (3)	X .25	117	$> 1000^\circ \text{K}$
4	2.6:1	0.26	475 (1)	X 1	27	$\approx 85^\circ \text{K}$
4	2.6:1	0.26	475 (1)	X .5	34	$\approx 130^\circ \text{K}$
4	2.6:1	0.26	475 (1)	X .25	45	$\approx 250^\circ \text{K}$
4	2.6:1	0.26	475 (1)	X .25	45	$\approx 250^\circ \text{K}$
4	2.6:1	0.26	680 (3)	X 1	56	$\approx 500^\circ \text{K}$
4	2.6:1	0.26	680 (3)	X .5	69	$\approx 700^\circ \text{K}$
4	2.6:1	0.26	680 (3)	X .25	92	$> 1000^\circ \text{K}$

Notes:

1 = operating current

2 = operating current + 10 %

3 = quench current

* = recommended design

temperature, but the difference between the two cables, 10% to 15% in the region of interest (above $50 KI^2dt$), is not large. It is desirable that maximum coil temperatures should be in the range 400 K – 500 K.

The growth of the resistive region in a magnet is a complex process. Quench propagation along a single conductor is determined by the distance of the conductor from the critical surface (H_c , T_c , J_c), the resistivity of the copper, and heat transfer to the adjacent medium (e.g., helium). Quench propagation to adjacent turns, radially or azimuthally, is determined by the heat capacities of the insulation and other components, such as fiberglass and epoxy. For this study, measurements from a helical magnet have been used to approximate the growth of resistance versus time in the SCQ magnet. Resistance will increase more slowly with time in the SCQ than in the helical magnet since the pole tip field in the SCQ is $\sim 2\text{T}$, while the central field in the helical dipoles is $\sim 4\text{T}$. This effect is approximated by scaling the helical magnet measurement by 0.5 and 0.25.

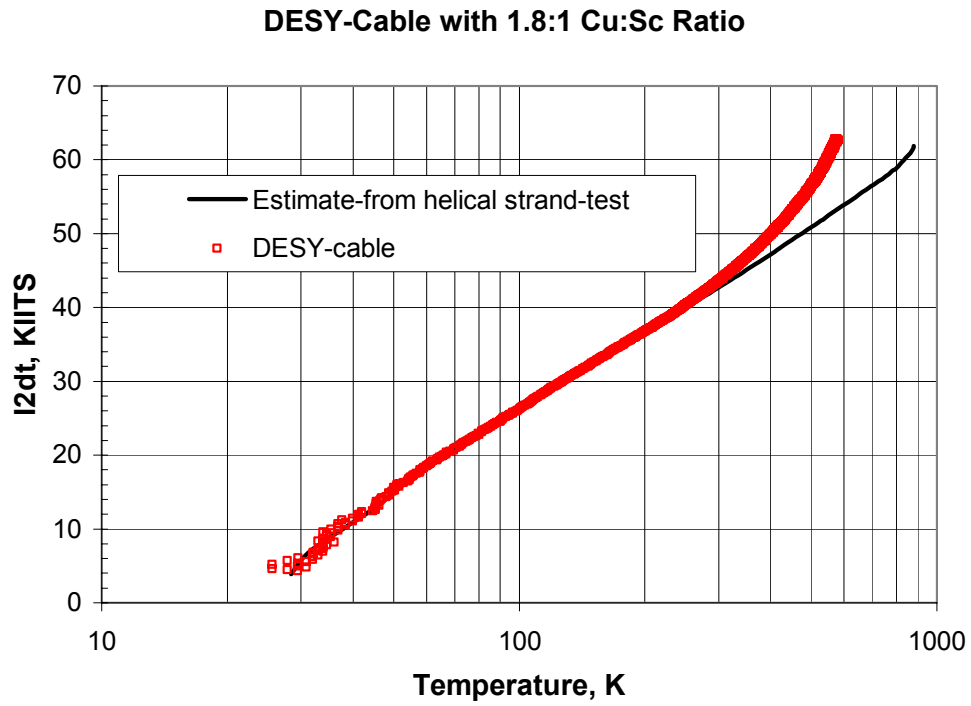


Figure A1.1: Measured Properties for DESY Cable used for HERA-II Magnets.

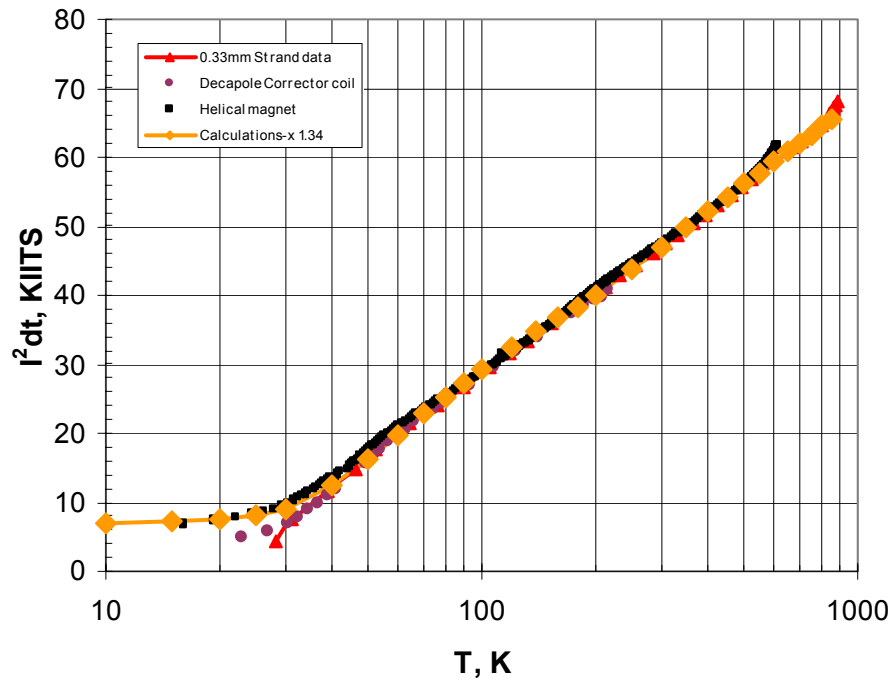


Figure A1.2: Measured Properties for Helical Cable with 2.5:1 Cu:Sc Ratio.

$$(((T-.02)*(T>.02)*(T<=.04))+(((8*T)-.28)*(T>.04)*(T<=.06))+(((20*T)-1.0)*(T>.06)*(T<=.08))$$

$$+(((50*T)-3.4)*(T>.08)*(T<=.1))+(((170*T)-15.4)*(T>.1)*(T<=.12))+5*(T>.12))*0.25$$

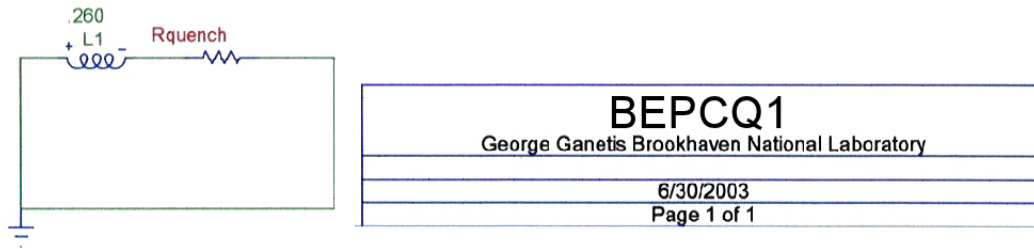


Figure A1.3: BEPC-II SCQ Quench Model.

To scale from the measurements of the helical magnet to the four options for SCQ, the magnets were modeled as a simple circuit (inductor and resistor in series) in a circuit analysis program (Micro-Cap 6), as shown in Figure A1.3. The model was used to separate the inductive and resistive voltages in the helical magnet and then to calculate the current decay in the SCQ for the same function of resistance versus time and for this function scaled by 0.5 and 0.25. The results of one calculation are given in Figure A1.4. In this figure, the horizontal axis is time from the start of the quench to 500 ms. The variables plotted, from the top to the bottom, are current (A), KL^2dt , and resistance (ohms). (Beyond ~ 120 ms, the growth of resistance matters little, and it is capped at 5 ohms beyond this time.)

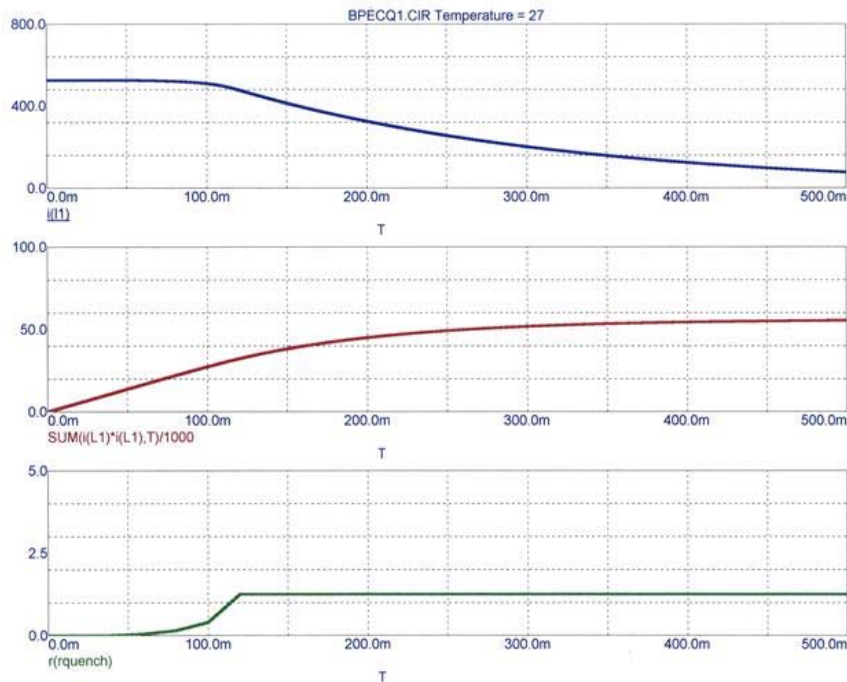


Figure A1.4: BEPC-II SCQ Quench Calculation Plots.

The calculated KI^2dt results, and the corresponding temperatures, for SCQ wound with three double layers are given in Table A1.1. (Since the cables are similar, the same $R(t)$ function is used for both 1.8:1 and 2.5:1 cables, yielding the same KI^2dt results for the same current. The conductor temperatures are determined from Figures A1.1 and A1.2 and are slightly different for the two cables.) Table A1.2 presents the same results for a SCQ wound with four double layers.

Recommendations.

For the region of interest, there is not a significant difference between the quench propagation properties of the two cables (1.8:1, 2.5:1). However, 1.8:1 conductor has a larger temperature margin than 2.5:1 conductor. This suggests choosing conductor with a copper-to-superconductor ratio of 1.8:1.

Since there will be no prototypes for the magnets, a more conservative approach should be adopted when possible. In comparing the three double-layer and four double-layer designs, one is comparing the effect of larger current (which enters as I^2) in the three double-layer coil with the effect of larger inductance (which enters as L) in the four double-layer coil. For quenches at operating current, with 1.8:1 cable, and using the most conservative scaling factor (0.25), the final temperature in the three double-layer coil is ~550 K whereas in the four double-layer coil it is ~330 K. This suggests choosing the coil with four double-layers.

Appendix 2. Power Supply, Instrumentation and Quench Protection

Considerations

The BEPCII superconducting magnets will require active protection from quenches. The quench of a superconducting magnet occurs when the superconducting wire is subjected to conditions exceeding the superconductor's capabilities. This may occur as a result of excessive temperature, current, or magnetic field at some point within the magnet. When a quench occurs, the superconductor loses its ability to transfer current without resistive losses. The current densities within the superconductors are large enough that resistive losses during operation will very quickly damage the magnet through the generation of heat.

A quench event can be produced by internal magnet issues, or by external influences. Externally, the magnetic field of the detector solenoid is capable of upsetting the magnet conductors. This can occur by ramping the solenoid too quickly, either up or down, or making the external field too large. Additionally, the beam itself carries enough energy to quench the magnet, and may do so should the beam collide with any of the magnet components.

To protect the BEPCII magnets, the first step is the detection of a quench event. Two methods may be used to determine the start of a resistive zone within a magnet.

1. Voltage taps: The BEPCII magnets will contain voltage tap points at all the necessary locations for monitoring every coil within the magnet. With a voltage tap at the end of each coil, and one in the center, it is possible to measure the difference between halves of a coil. When a coil is powered, either steady state or during ramping, the two coil halves will have almost identical voltages present across them, as seen at the voltage taps. Should a quench occur in one of the coil halves, the quench region will develop a voltage drop across the normal zone, and this additional voltage will be sensed by the quench detector electronics. The BEPCII system will require continuous monitoring of 28 coil half signals, 24 superconducting bus signals, 24 gas cooled leads, and 15 power supply current signals.
2. Current derivative: The rate of change of power supply current is calculated, and the inductive voltage across the magnet is compared to the calculated voltage.

To monitor the voltage taps for quench detection, a Digital Signal Processing (DSP) based system is recommended. This type of system provides system flexibility, allowing programming changes to accommodate operational modifications, and provides the ability to data log in real time, needed for troubleshooting the system.

Once a quench has been detected, several things must be done. First, the power supplies feeding all the magnet circuits must be shut down. Second, the energy must be extracted from the magnet. The speed at which the energy can be removed from the

BEPC-II Superconducting Magnet Electrical Circuits

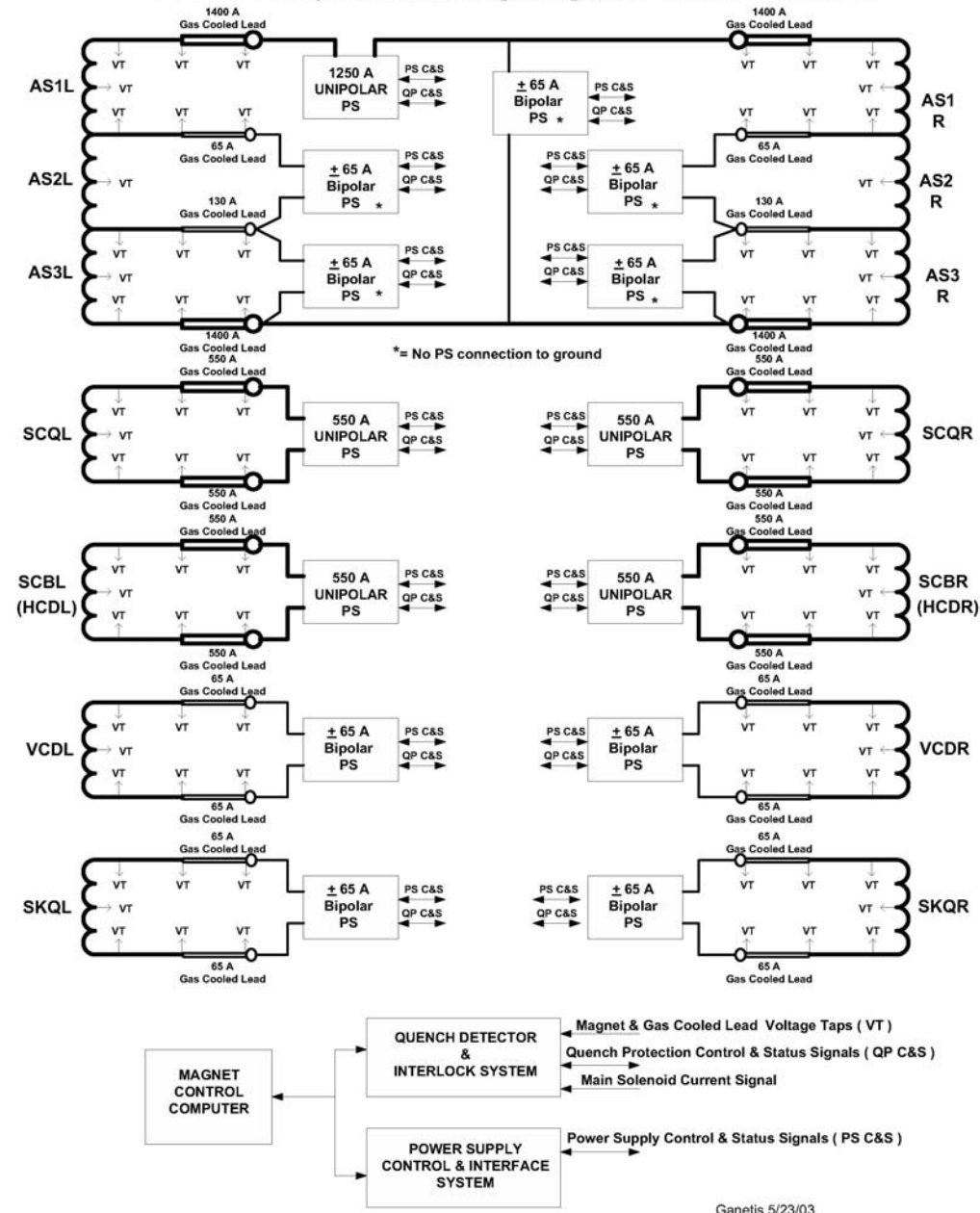
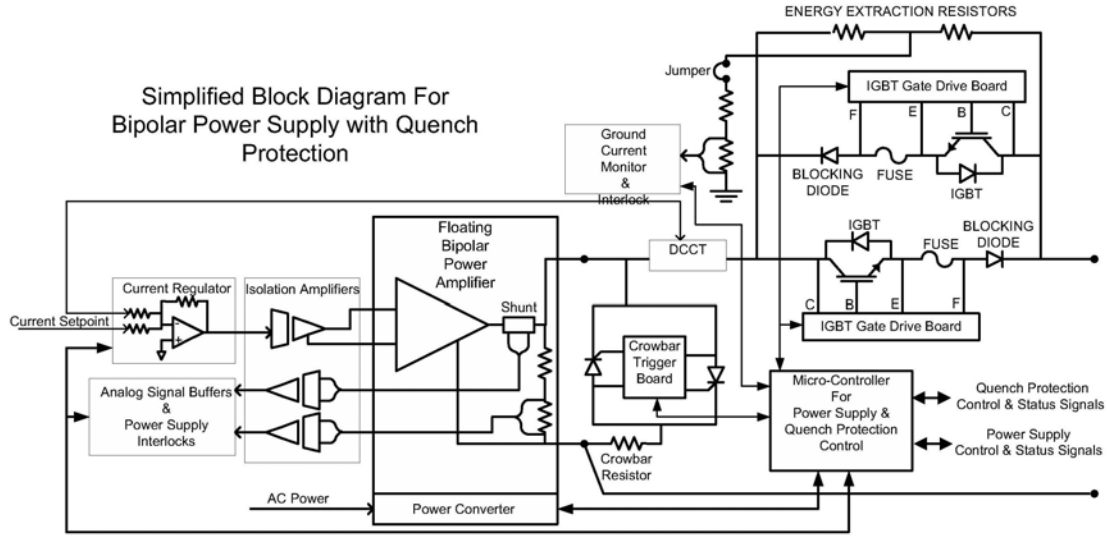


Figure A2.1: BEPC-II Superconducting Magnet Electrical Circuit.

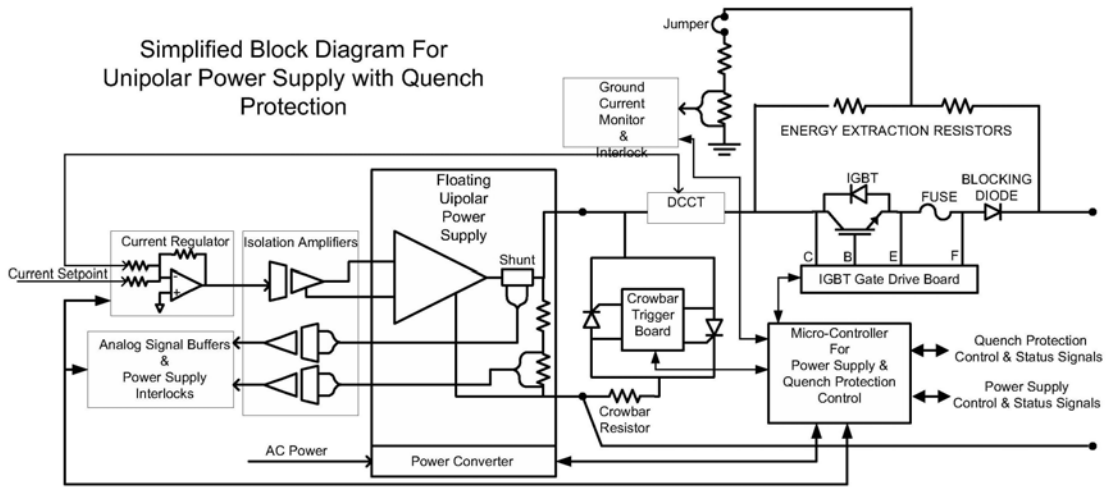
magnet will depend on the highest voltage that may be safely placed across the magnet. The higher the voltage, the faster will be the energy extraction. This energy will be dissipated within a resistor external to the magnet.

The power supply and quench protection system, in simplified form as seen in Figure A1.1, details the configuration required for powering the magnet as well as turning it off quickly to avoid damage.



Ganetis 5/23/03

Figure A2.2: Bipolar Power Supply with Quench Protection.



Ganetis 5/23/03

Figure A2.3: Unipolar Power Supply with Quench Protection.

RHIC TYPE QUENCH DETECTION SYSTEM BLOCK DIAGRAM

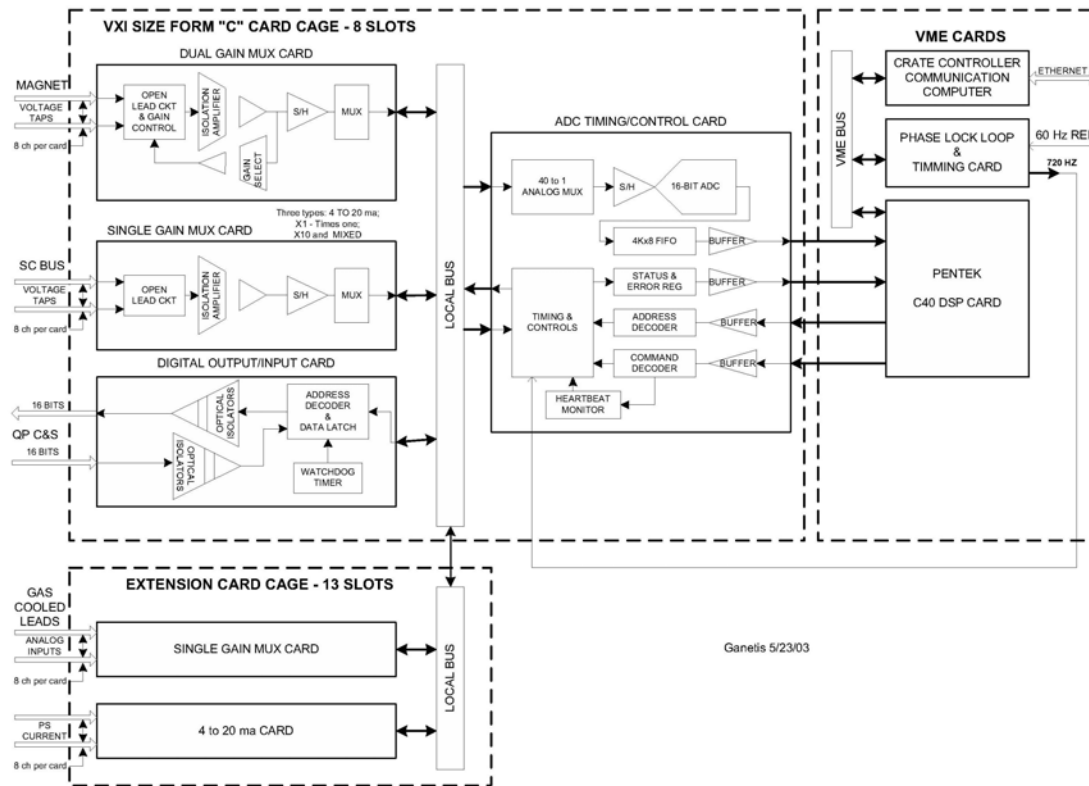


Figure A2.4: RHIC Type Quench Detection Block Diagram.

When a quench is detected, this supply configuration will safely turn off all supplies, and divert the stored energy within the magnet to external dump resistors.

Appendix 3. Drawing Package and Parts List

The following is a master list of parts for the BNL BEPC-II Superconducting IR magnet. The list is organized numerically and by levels within the magnet assembly. The overall magnet assembly is listed below as level "0". All other parts listed as level "1" report directly to the main magnet assembly. All other parts listed as level "n" report to the level "n-1" subassembly directly above them. Renderings of 3-Dimensional models of the main magnet assembly and major subassemblies appear below the list. Electronic files in AutoCad drawing format of all parts are included on an accompanying compact disc.

MULTI-LEVEL MASTER PARTS LIST
PART NUMBER: 21010001 REV 0, PLREV 0
DESCRIPTION: ASSY, BNL BEPC-II MAGNET

LEVEL	PART NUMBER	DESCRIPTION	QTY	UOM
0	21010001	ASSY, BNL BEPC-II MAGNET		ea
1	12010441-01	FILLER WIRE, WELDING	As req'd	LB
1	21010002	FRONT PLATE WELDMENT	1.0000	ea
2	21010007	ASSY, FLANGE WELDMENT	1.0000	ea
3	21010013	TUBE, FRONT FLANGE	1.0000	ea
3	21010014	FLANGE	1.0000	ea
3	21010069	ALUMINUM WELDING ROD	As req'd	ea
2	21010011	FRONT PLATE, MACHIN	1.0000	ea
2	21010069	ALUMINUM WELDING ROD	As req'd	ea
2	21010077	RELIEF VALVE HOUSIN	1.0000	ea
1	21010003	ASSY, WIRING BOX	1.0000	ea
2	12010441-01	FILLER WIRE, WELDING	As req'd	LB
2	21010024	HOUSING, WIRING BOX	1.0000	ea
2	21010025	BASE, WIRING BOX	1.0000	ea
2	21010026	PIPE, OUTLET, WIRING	1.0000	ea
2	21010028	FLANGE, SMALL, WIRI	1.0000	ea
2	21010048	FLANGE, WIRING BOX	1.0000	ea
2	21010051	MOUNTING BLOCK, WIRING	1.0000	ea
1	21010004	ASSY, COIL SUPPORT	1.0000	ea
2	12010441-01	FILLER WIRE, WELDING	As req'd	LB
2	21010018	TUBE, COIL SUPPORT	1.0000	ea
2	21010023	END CAP, LE	1.0000	ea
1	21010005	ASSY, OUTER NITROGEN	1.0000	ea
2	12010441-01	FILLER WIRE, WELDING	As req'd	LB
2	21010041	SHIELD, NITROGEN	1.0000	ea
2	21010055	TUBE, NITROGEN, OUT	8.0000	ea
1	21010006	ASSY, INNER NITROGEN	1.0000	ea
2	12010441-01	FILLER WIRE, WELDING	As req'd	LB
2	21010043	SHIELD, NITROGEN	1.0000	ea
2	21010053	TUBE, NITROGEN	8.0000	ea
2	21010059	MANIFOLD, NITROGEN	1.0000	ea

LEVEL	PART NUMBER	DESCRIPTION	QTY	UOM
1	21010008	ASSY, HELIUM CONTAIN	1.0000	ea
2	12010441-01	FILLER WIRE, WELDING	As req'd	LB
2	21010020	TUBE, HELIUM	1.0000	ea
2	21010039	RETAINING BRACKET,	8.0000	ea
2	21010040	RETAINING PAD, TUBE	8.0000	ea
1	21010010	HOUSING, END VOLUME	1.0000	ea
1	21010012	REAR PLATE	1.0000	ea
1	21010015	CRYOSTAT TUBE	1.0000	ea
1	21010016	BEAM TUBE	1.0000	ea
1	21010017	TUBE	1.0000	ea
1	21010019	COIL	1.0000	ea
1	21010021	END CAP, NLE	1.0000	ea
1	21010022	END HOUSING	1.0000	ea
1	21010029	COVER, WIRING BOX	1.0000	ea
1	21010033	SUPPORT POST, LONG	3.0000	ea
1	21010034	SUPPORT POST, SHORT	3.0000	ea
1	21010038	RETAINING KEY, TUBE	8.0000	ea
1	21010045	AXIAL RESTRAINT	1.0000	ea
1	21010046	COMPRESSION PLATE	1.0000	ea
1	21010047	COMPRESSION PLATE	1.0000	ea
1	21010052	TUBE, WIRING BOX	1.0000	ea
1	21010056	MANIFOLD, NITROGEN,	1.0000	ea
1	21010057	MANIFOLD, NITROGEN,	1.0000	ea
1	21010058	END CAP, NITROGEN M	2.0000	ea
1	21010072	BELLOWS ASSY	1.0000	ea
2	21010035	BELLOWS	1.0000	ea
2	21010036	BELLOWS FLANGE, IN	1.0000	ea
2	21010037	BELLOWS FLANGE, OUT	1.0000	ea
1	21010080	ASSY, FLEXIBLE HOSE	1.0000	ea
2	12010441-01	FILLER WIRE, WELDING	As req'd	LB
2	21010060	HOSE, FLEXIBLE, MOD	1.0000	ea
3	21010070	HOSE, FLEXIBLE	1.0000	ea
2	21010062	TUBE, FLEXIBLE HOSE	1.0000	ea
2	21010065	TUBE, FLEXIBLE HOSE	1.0000	ea
2	21010067	FLANGE, ROTATABLE	1.0000	ea
2	21010071	INSERT, ROTATABLE	1.0000	ea
1	21010081	ASSY, FLEXIBLE HOSE	1.0000	ea
2	12010441-01	FILLER WIRE, WELDING	As req'd	LB
2	21010060	HOSE, FLEXIBLE, MOD	1.0000	ea
3	21010070	HOSE, FLEXIBLE	1.0000	ea
2	21010063	TUBE, FLEXIBLE HOSE	1.0000	ea
2	21010067	FLANGE, ROTATABLE	1.0000	ea
2	21010071	INSERT, ROTATABLE	1.0000	ea
1	21010082	ASSY, FLEXIBLE HOSE	1.0000	ea
2	12010441-01	FILLER WIRE, WELDING	As req'd	LB
2	21010060	HOSE, FLEXIBLE, MOD	1.0000	ea
3	21010070	HOSE, FLEXIBLE	1.0000	ea
2	21010061	TUBE, FLEXIBLE HOSE	1.0000	ea
2	21010067	FLANGE, ROTATABLE	1.0000	ea
2	21010071	INSERT, ROTATABLE	1.0000	ea
1	DIN912A4M8X45	SCR,CAP,SCH, M8X1.2	As req'd	EA

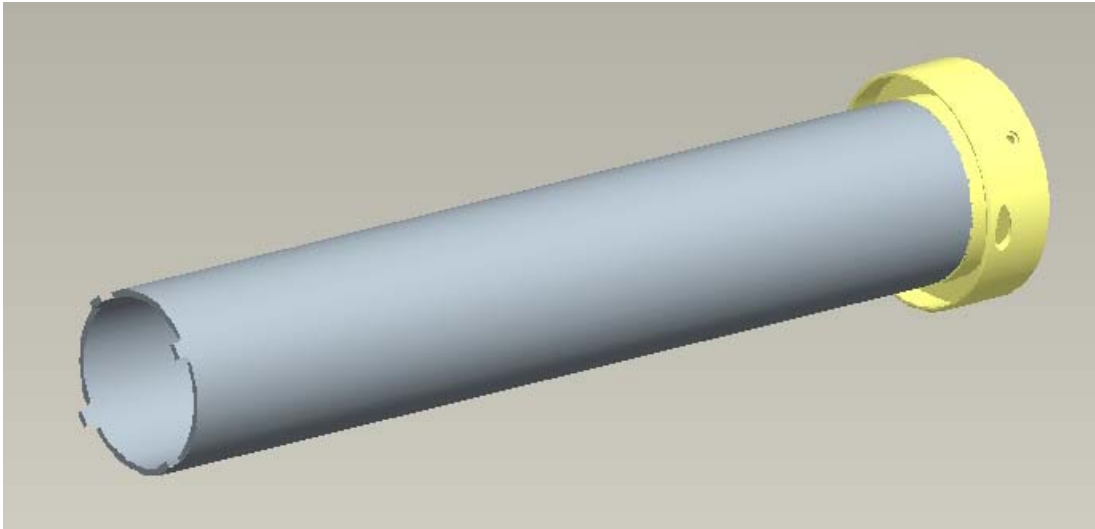


Figure A3.1: Coil Support Tube Assembly. *Notches at IP end for radial helium passage between inner and outer flow annuluses, and flange pre-welded onto non-IP end are shown.*

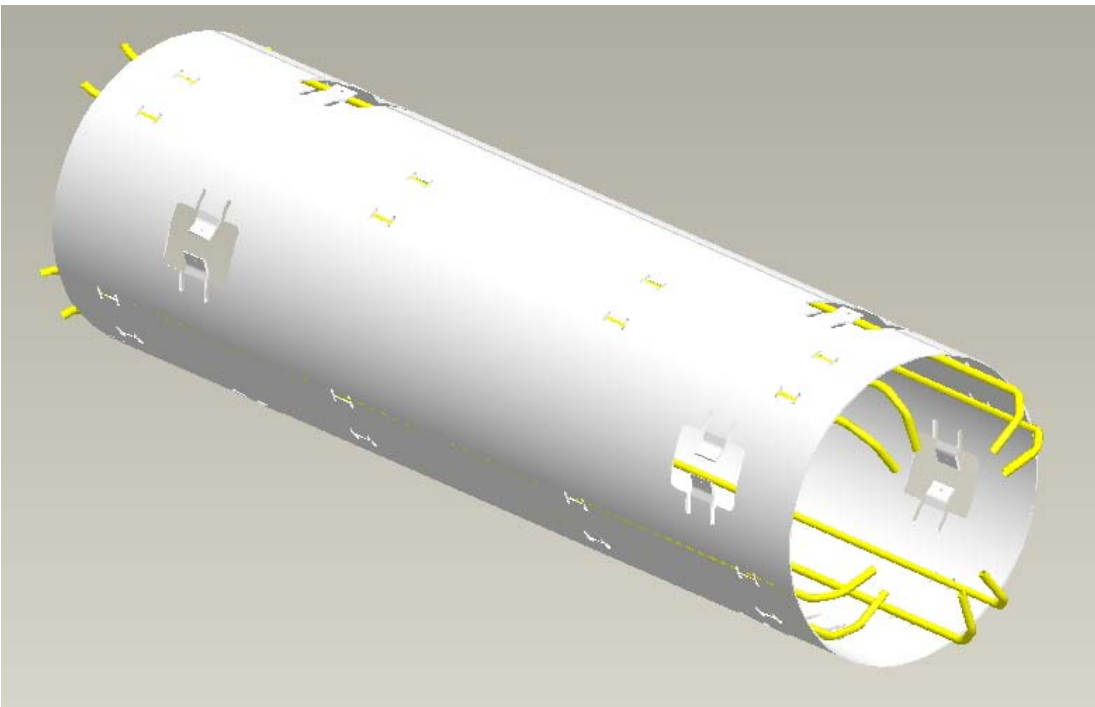


Figure A3.2: Outer Heat Shield Assembly. *Helium lines that are welded in place and tabs for mechanical heat stationing of magnet supports are shown.*

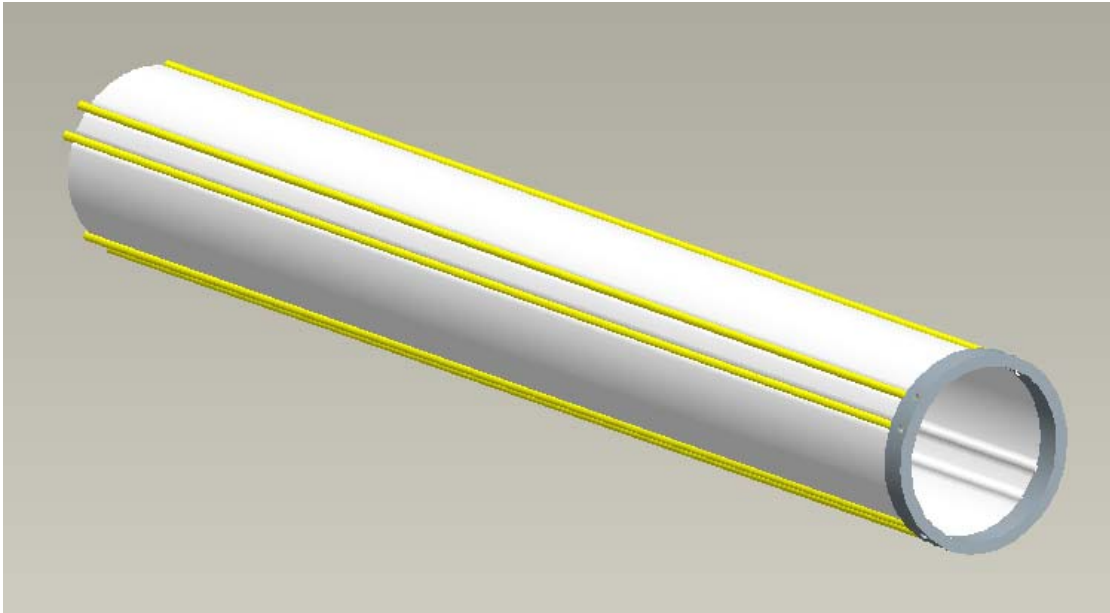


Figure A3.3: Inner Heat Shield Assembly. *Helium lines that are welded in place and the end manifold are shown.*

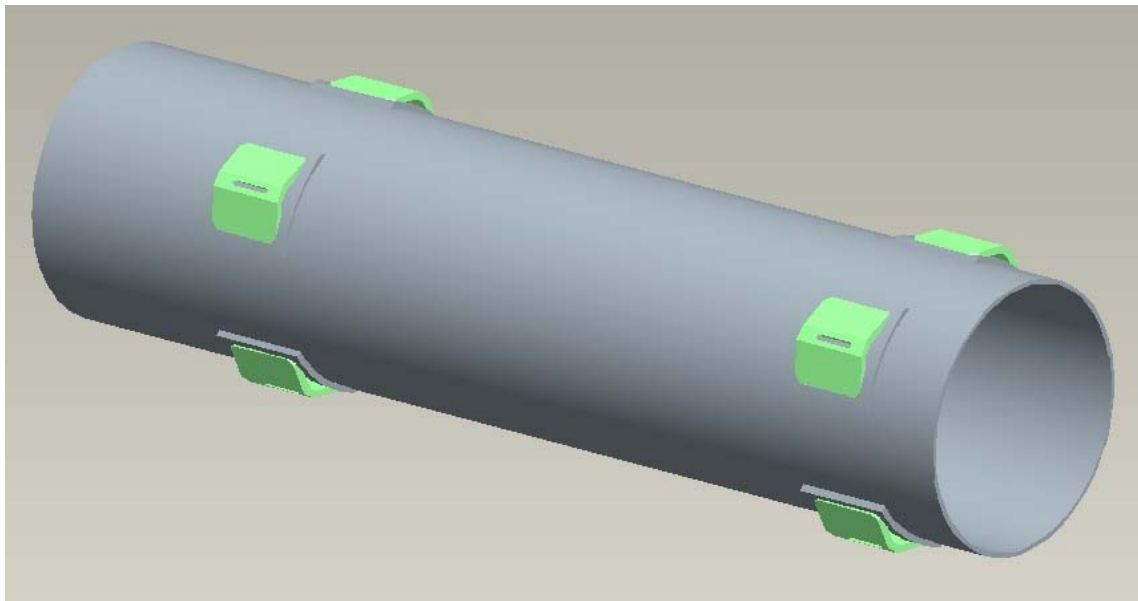


Figure A3.4: Helium Containment Tube Weldment. *G-10 magnet supports that are held in place by welded stainless steel retainers are shown.*



Figure A3.5: Bellows Assembly. *The bellows assembly was recently increased in size to provide requested clearance volume of $\text{Ø}190\text{mm} \times 50\text{mm}$ at non-IP end.*